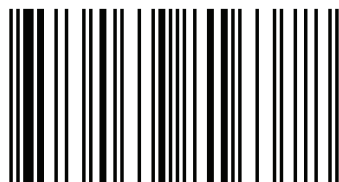


During the recent years, it was occurred a large number of natural disasters throughout the world. One of the major reasons behind this is the disturbance in the equilibrium of the natural ecosystems. Deforestation can be identified as a main anthropogenic activity causing destruction of the natural environment. So, the studies on the deforestation have become a timely topic. Sri Lanka is one of the few remaining countries in the world with extensive natural forest cover, but much of the existing forests have been destroyed, mainly by shifting cultivation, logging and by the growth of number of people involved in agriculture. Therefore, the magnitude of deforestation and its consequences on natural processes need to be investigated. So, an attempt was taken in this research to understand the changes in forest cover throughout the study area using Microwave Remote Sensing techniques. The study area was selected in the Wilpattu National Park in Sri Lanka, because the area is highly deforested due to the human activities.



Prasadi Thilanka Senadeera
Duminda Ranganath Welikanna

Estimates the Forest Canopy Loss using Space Borne C Band SAR Images



978-613-9-81637-8

**Prasadi Thilanka Senadeera
Duminda Ranganath Welikanna**

**Estimates the Forest Canopy Loss using Space Borne C Band SAR
Images**

**Prasadi Thilanka Senadeera
Duminda Ranganath Welikanna**

**Estimates the Forest Canopy Loss
using Space Borne C Band SAR
Images**

Imprint

Any brand names and product names mentioned in this book are subject to trademark, brand or patent protection and are trademarks or registered trademarks of their respective holders. The use of brand names, product names, common names, trade names, product descriptions etc. even without a particular marking in this work is in no way to be construed to mean that such names may be regarded as unrestricted in respect of trademark and brand protection legislation and could thus be used by anyone.

Cover image: www.ingimage.com

Publisher:

LAP LAMBERT Academic Publishing

is a trademark of

International Book Market Service Ltd., member of OmniScriptum Publishing

Group

17 Meldrum Street, Beau Bassin 71504, Mauritius

Printed at: see last page

ISBN: 978-613-9-81637-8

Copyright © Prasadi Thilanka Senadeera, Duminda Ranganath Welikanna

Copyright © 2018 International Book Market Service Ltd., member of

OmniScriptum Publishing Group

All rights reserved. Beau Bassin 2018

To my loving parents for their unconditional love, inspiration, strength and courage you gave me throughout my life, the dreams come true because of you!

Miss. K.H.P.T. Senadeera

Demonstrator

Prasadi.senadeera@geo.sab.ac.lk

Qualifications

Bachelor of Surveying Sciences (Photogrammetry & Remote Sensing), Sabaragamuwa University, 2017

Profile

K.H. Prasadi T. Senadeera is currently employing as a Demonstrator in the Department of Remote Sensing and GIS of the Faculty of Geomatics, Sabaragamuwa University of Sri Lanka. She could complete her degree with a first class honors and furthermore there she was able to award with a gold medal for the best performance and the highest final grade point average of the Faculty of Geomatics.

Research interests

Radar image analysis and interferometry

Hyperspectral Image analysis

Uncontrolled urbanization effects on natural eco systems

Land Surveying applications

Dr. DR Welikanna

Senior Lecturer

drw@geo.sab.ac.lk

Qualifications

PhD in Geoinformatics, Department of Civil and Earth Resources Engineering, Kyoto University, 2014

MSc in Geoinformatics, Department of Earth Observation Science, University of Twente, 2008

Bachelor of Surveying Sciences, Sabaragamuwa University, 2004

Profile

Duminda R Welikanna is currently a Senior Lecturer at the Department of Surveying and Geodesy, Faculty of Geomatics. He is presently the Head of the Department of Surveying and Geodesy and the Research Co-coordinator for the Faculty of Geomatics. He has been awarded the Japanese Government Scholarship 2011 and the Sri Lanka Parliamentary Scholarship for Engineering 2006.

Research Interests

Image analysis: classification, segmentation

Super resolution Mapping (Markov Random Fields)

Radar image analysis and Radar interferometry

Dr. HMI Prasanna

Senior Lecturer

indika@geo.sab.ac.lk

Qualifications

Doctor of Philosophy, the Hong Kong Polytechnic University, Hong Kong

MPhil in Geodesy, University of Sri Jayewardenepura, Sri Lanka

BSc in Surveying Sciences, Sabaragamuwa University of Sri Lanka

Profile

Dr. H.M.I.Prasanna is a Senior Lecturer (Gr. I) at the Department of Surveying and Geodesy, Faculty of Geomatics, Sabaragamuwa University of Sri Lanka. He is also a visiting lecturer at the University of Sri Jayewardenepura and General Sir John Kotelawala Defence University. Mainly he is teaching Geodesy and Geodetic Reference Systems for undergraduate and postgraduate students. Presently he is the Dean of the Faculty of Geomatics and the member of the University Council and the Senate. His research focuses on gravity field modeling and geodetic datum.

Research Interests

Earth gravity field modeling

Geodetic reference systems and Datums

Internal structure of Earth

Abstract

Deforestation could be identified as one of the main anthropogenic agent leading to an imbalance in the natural ecosystems triggering disasters in the form of landslides, floods and droughts. Recent studies show that Earth Observation (EO) data offer new opportunities for fast, reliable and accurate deforestation detection at smaller scales. Synthetic aperture radar (SAR) data has huge potential in terms of its scattering mechanism and all whether capabilities to estimate the forest canopy loss as an indirect measure of deforestation. A region that has been subjected to heavy deforestation during the past few years in North West region of Sri Lanka was focused for this experiment. Time series single polarized (VV) Sentinel-1 C band SAR data was employed in this study. The low canopy penetration capabilities of C Band SAR systems were significantly utilized in the study. Two Sentinel-1 VV polarization interferometric wide swath (IW) images from the year 2015 and 2016 covering the heaviest deforestation period of the study area were used. These images were carefully preprocessed in order to extract the backscatter intensity to perform the change detection. Coherence based change detection and Image rationing were performed to estimate the canopy loss primarily. Further analysis has been carried out in order to intensify the backscatter difference using radar texture. Second order texture measures, Homogeneity, Entropy and Angular Second Moment (ASM) were identified to give the highest correlation with the changes derived from complex coherence and image rationing. Both Coherence and Backscatter values for deforested regions are lower than those of regions with forest cover. Experimental results suggest that the Homogeneity texture has the advantage in delineating the difference between the forest and bare soil classes. The comparative results between the ground truth based referenced images generated from Google images and the SAR texture based interpretation suggests that an alarming area of 0.0207886 km^2 has been changed from forest to soil.

KEY WORDS: SAR, Change detection, Coherence, Backscatter, Texture, GLCM

Table of contents

1. Introduction	2
1.1. Background	2
1.1.1. Forest.....	2
1.1.2. Forest in Sri Lanka.....	2
1.2. Deforestation.....	3
1.2.1. Deforestation in Sri Lanka	4
1.3. Remote Sensing applications in Forestry.....	5
1.4. Research problem.....	6
1.5. Objectives.....	6
1.5.1. Main Objective:	6
1.5.2. Minor Objectives:	6
1.6. Scope and limitations	6
2. Literature Review	7
2.1. Microwave Remote Sensing for Forest Applications.	7
2.1.1. Radar wavelength and polarization for forest applications	7
2.2. Scattering mechanism of forest	8
2.2.1. Scattering types in forests	9
2.3. Scattering mechanism in C band.....	11
2.3.1. C band SAR.....	11
2.4. Change Detection using SAR data	11
2.4.1. Complex Coherence Estimation.....	12
2.4.2. Image Differencing	13
2.4.3. Image Rationing	13
2.4.4. Correlation coefficient	14
2.4.5. Texture Analysis	14
2.4.5.1. Mean Texture	15
2.4.5.2. Standard Deviation texture measure	15
2.4.5.3. Grey Level Co-occurrence Matrix	15

3. Theoretical background.....	17
3.1. Remote Sensing.....	17
3.1.1. Remote sensing in forestry applications	17
3.2. Classification of Remote Sensing systems according to the energy source.....	18
3.2.1. Passive systems	18
3.2.2. Active systems	18
3.3. Classification of remote sensing systems with respect to the wave length.....	18
3.3.1. Optical remote sensing.....	18
3.3.2. Microwave Remote Sensing	19
3.4. RADAR remote sensing for forest applications.....	19
3.5. RADAR	20
3.5.1. Real Aperture Side-looking Airborne Radar (SLAR).....	21
3.5.2. Synthetic Aperture Radar (SAR)	21
3.5.3. Basic principle of RADAR	21
3.5.4. RADAR image geometry	22
3.5.4.1. Intensity.....	22
3.5.4.2. Phase	22
3.5.5. RADAR Image Resolutions	23
3.5.5.1. Azimuth Resolution	23
3.5.5.2. Range Resolution.....	24
3.5.6. RADAR viewing Geometry	25
3.5.6.1. Incidence angle (θ)	25
3.5.6.2. Look angle.....	26
3.5.6.3. Near Range and Far Range	26
3.5.6.4. Slant Range and Ground range	26
3.5.7. Geometric distortions on RADAR images.....	27
3.5.7.1. Scale distortions.....	27
3.5.7.2. Relief Displacement.....	27
3.5.7.3. Layover	28

3.5.7.4. Fore shortening	28
3.5.7.5. Shadow.....	29
3.5.7.6. Speckles	29
3.5.8. RADAR Waveform Properties	30
3.5.8.1. Wavelength and Frequency.....	30
3.5.8.2. Amplitude	31
3.5.8.3. Polarization	31
3.5.9. RADAR equation.....	31
3.5.10. RADAR Backscatter	32
4. Study area and Data.....	33
4.1. Study Area.....	33
4.2. Data	34
4.2.1. Sentinel I Mission	34
4.2.2. SENTINEL-1 operating modes.....	35
4.2.3. Sentinel 1 data products	36
4.2.4. Description about used Data	37
4.2.5. Auxiliary Data Sets	37
4.2.6. Tools Used	37
5. Methodology	38
5.1. Acquiring Sentinel 1 (SLC) data.....	38
5.2. The flow chart of the methodology of this study	40
5.3. Preprocessing of Sentinel 1 Satellite Images	41
5.3.1. Apply orbit files	41
5.3.2. De burst	41
5.3.3. Multilooking.....	42
5.3.4. Geocoding (Range Doppler Terrain Correction)	43
5.3.5. Co registration.....	44
5.3.6. Subset	45
5.4. Graph builder	45
5.4.1. Graph of pre-process an image	45

5.5.	Extraction of deforested areas from RADAR images.....	46
5.5.1.	Graph for Coherence estimation	46
5.5.2.	Graph for Change detection by image rationing.....	47
5.5.3.	The correlation coefficient.....	47
5.6.	Texture Analysis	50
	Graph for Texture Analysis by GLCM	50
6.	Rsults and Discussion.....	51
6.1.	Coherence Estimation.	51
6.2.	Change detection Estimation.....	57
6.3.	Teture Analysis	61
6.3.1.	MATLAB processing for texture analysis.....	62
6.3.2.	GLCM Analysis	63
6.4.	Correlation coefficient	68
7.	Conclusion.....	71
8.	Reference.....	72

List of figures

Figure 1 : Forested areas	2
Figure 2: Deforested area	3
Figure 3: Changes of forest cover in Sri Lanka between 1992 and 2010 (REED+ Sri Lanka, 2007)	5
Figure 4: Penetration of different wave length in canopy (Vyjayanthi N.V., 2008).	8
Figure 5: Scattering types in forests.....	10
Figure 6: Active and Passive remote sensing systems	18
Figure 7: Regions of the electromagnetic spectrum that are of interest in remote sensing applications (Mather M.P., 2009).....	19
Figure 8: Radar working principle	21
Figure 9: RADAR viewing geometry (http://www.nrcan.gc.ca , 2017).	25
Figure 10: The relationship between radar incident angle θ true vertical and local slope angle (a) for non-level terrain (http://www.nrcan.gc.ca , 2017)	25
Figure 11: Slant range and Ground range of RADAR system (http://www.nrcan.gc.ca , 2017).....	26
Figure 12: Slant range scale distortion (http://www.nrcan.gc.ca , 2017).....	27
Figure 13: Layover effect on RADAR images (Mather M.P., 2009).....	28
Figure 14: foreshortening and shadow in RADAR images (Mather M.P., 2009).....	28
Figure 15: Relationship between Geometric distortions and incidence.....	29
Figure 17: RADAR image with speckles (Mather M.P., 2009)	30
Figure 17: RADAR image without speckles (Mather M.P., 2009).....	30
Figure 18: RADAR Wave form properties (Mather M.P., 2009)	31
Figure 19: Location of Wilpattu National Park (Not to Scale)	33
Figure 20: SENTINEL-1 Constellation.....	34
Figure 21: SENTINEL-1 Operating Modes (https://sentinel.esa.int/ , 12.05.2017).	35
Figure 22: Scientific Hub selection window	38
Figure 23: Displayed data sets for selected area.	39
Figure 24: Flow chart for the Methodology	40
Figure 25: Apply orbit files	41
Figure 26: Before the Deburst	41
Figure 27: After the Deburst	41
Figure 28: Before the Multilooking	42
Figure 29: After the Multilooking.....	42
Figure 30: After the Range Doppler Terrain Correction.....	43
Figure 31: Before the Range Doppler Terrain Correction	43
Figure 32: Overview of Coregistration Processing Chain	44
Figure 33: Geocoded Product.....	44

Figure 34: Subset tool	45
Figure 35: Image preprocessing steps in a single Graph operation.....	45
Figure 36: Coherence estimation.....	46
Figure 37: change detection by image rationing	47
Figure 38: Statics for subset of 2016.09.26 image	48
Figure 39: Statics for subset of 2015.06.24 image	48
Figure 40: Correlation coefficient by Band Math operator.....	49
Figure 41: Band Math operator	49
Figure 42: Graph for Texture analysis	50
Figure 43: Coherence between images of 2016.06.04 and 2016.08.15 (VV Polarization) [1, 2].....	51
Figure 44: Coherence between images of 2016.06.04 and 2016.07.16 (VV Polarization) [1, 5].....	51
Figure 45: Coherence between images of 2016.03.18 and 2016.09.26 (VH Polarization) [1, 2].....	51
Figure 46: Coherence between images of 2016.06.04 and 2016.08.16 (VV Polarization) [1, 6].....	51
Figure 47: Low forest cover	52
Figure 48: Water.....	52
Figure 49: Deforested area	53
Figure 50: Dense forest cover	53
Figure 51: Histogram for dense forest cover.....	53
Figure 52: Histogram for moderate forest cover	54
Figure 53: Histogram for Water	54
Figure 54: Histogram for Deforested area.....	54
Figure 55: Mean coherence value for selected regions	55
Figure 56: Histogram for Coherence.....	56
Figure 57: Change detection between images of 2016.06.04 and 2016.08.15 (VV Polarization) [1, 2]	57
Figure 58: Change detection between images of 2016.06.04 and 2016.07.16 (VV Polarization) [1, 5]	57
Figure 59: Change detection between images of 2016.06.04 and 2016.08.09 (VV Polarization) [1, 6]	57
Figure 60: Change detection between images of 2016.03.18 and 2016.09.26 (VH Polarization) [1, 2]	57
Figure 61: Histogram for Dense forest.....	58
Figure 62: Histogram for Low forest Cover.....	58
Figure 63: Histogram for Water	59
Figure 64: Histogram for Deforested area.....	59
Figure 65: Mean backscatter for selected regions	60
Figure 66 : Google Earth image for selected deforested area	61
Figure 67: Subset of image 1 (2016.06.04)	62
Figure 68: Subset of image 6 (2016.08.09)	62
Figure 69: Standard Deviation texture of image 1 (2016.06.04)	62
Figure 70: Standard Deviation texture of image 6 (2016.08.09)	62

Figure 72: Mean texture of image 1 (2016.06.04)	63
Figure 72: Mean texture of image 6 (2016.08.09)	63
Figure 73: RGB Visualizations of Texture images derived for images acquired on 2015.06.04 and 2016.08.06.....	65
Figure 74: Area difference for different texture images	67
Figure 75: The correlation coefficient between subset of 2016.03.18 and 2016.09.26 (VH Polarization) [1, 2].....	68
Figure 76: The correlation coefficient between subset of 2015.06.04 and 2016.08.16 (VV Polarization) [1, 6].....	68
Figure 78: Extracted deforested areas from the scatter plot of Difference image for VH polarization pre and post images.....	69
Figure 78: Scatter plot between correlation coefficient and Difference image for VH polarization pre and post images.....	69

List of Tables

Table 1 Radar frequency and wave length	30
Table 2: Selected Sentinel 1 Data	37
Table 3: Coherence value for selected land use types	55
Table 4: Mean backscatter value of selected land use types.....	60
Table 5: Calculated area for different texture images	66
Table 6: The correlation between change detection methods and texture images.....	70

List of Abbreviations

CIA	Central Intelligence Agency
DEM	Digital Elevation Model
EC	European Commission
EMR	Electro Magnetic Radiation
ERS	European Remote-sensing Satellite
GLCM	Grey level co-occurrence matrix
IR	Infra-Red
IW	Interferometric Wide Swath
NPPD	National Protection and Programs Directorate
RADAR	Radio Detection and Ranging
RAR	Real Aperture Radar
SAR	Synthetic Aperture Radar
SLAR	Side Looking Airborne Radar
SONAR	Sound Navigation And Ranging
SRTM	Shuttle Radar Topography Mission
STD	Standard Deviation
TOPSAR	Topographic Synthetic Aperture Radar
UNDP	United Nations Development Programme
UTM	Universal Transverse Mercator
WGS	World Geodetic System

1. Introduction

1.1. Background

1.1.1. Forest

Forests cover 31% (FOA, 2010) of the land area on our planet. It is one of the most important renewable natural resources and has significant role in the human life and environment.

Forests play a major role in maintaining environmental balance on the earth. They have a prominent role in global carbon cycle, exchanging large fluxes of carbon with the atmosphere through the processes of photosynthesis, respiration and decomposition (Waring and Running, 1998).

Forest resources are



Figure 1 : Forested areas

important socially, economically and environmentally. Forest produces wood, protects wildlife, maintain groundwater levels, protect the soil fertility, and absorb carbon and another pollutant gases from the atmosphere. All these forest functions influence the continuity of life and have global implications (Heri *et al*, 1999) as well. Forests have traditionally been used for many products, including timber, fuel, and fodder.

1.1.2. Forest in Sri Lanka

Sri Lanka is an Island located in the Indian Ocean with the latitude of 9°50' - 5°50' in North and longitude of 79°10'- 82°5' in East Geographical Coordinates and has a tropical climate. The total area is 65,610 km² including 870 km² of water features and the terrain is mostly low, flat to

rolling plain which comprises 80% of the land area as well as the entire northern half of the island and continues around the coast to the southern half and mountains in south-central interior Sri Lanka rise to more than 2,133 meters (CIA, 2007).

Total forest area in Sri Lanka is 29.9% of the total land area while the primary forest cover is 2.6% of the total land area and the 8.6% of the total forest area. The forest area can be divided into primary forest, modified natural, and production plantation (Mongabay, 2006; Butler, 2006) until the turn of the 19th century Sri Lanka was almost entirely covered by tropical forests. Today only a fraction of these original old-growth forests remains. Deforestation is considered one of the most severe environmental issues in the country that threatens both humans and biodiversity and between 1990 and 2005, Sri Lanka was among the countries with the highest deforestation rates of primary forests in the world according to the Conservation International, 2011.

Since independence in 1948 the human population in Sri Lanka has tripled from 7 million to about 20.7 million in 2010. The population is unequally distributed over the island with much higher concentrations in the south-west, particularly around the capital city of Colombo, while the northern as well as eastern parts are less densely populated (UNDP, 2011, National encyclopedia, 2011).

1.2. Deforestation

Deforestation is the conversion of forest to another land use type which is mainly a result of human activities. In contrast, forest degradation leads to deterioration of the standing vegetation in density, structure and species composition due to human activities and natural causes. It may involve opening of the canopy, modification of the vertical structure, habitat parameters or change of other attributes. Forest degradation does not necessarily involve a reduction of the forest area, instead leads to the decline of the quality of forests. Together, deforestation and forest degradation reduce the area; quality and quantity of vegetation cover and alter the spatial structure of landscape through the process of fragmentation (Kariyawasam R. and Rajapakse C., 2002).



Figure 2: Deforested area

1.2.1. Deforestation in Sri Lanka

Sri Lanka is one of bio diversity hotspots (Conservation International, 2011). Most developments are destroying natural environment in Sri Lanka. While this development moves forward, environmental conditions are getting worse (Kariyawasam R. and Rajapakse C., 2002). About 200 years ago Sri Lanka was almost entirely covered by tropical forests. During the colonial period in forest areas got cleared in order to develop commercial agriculture. Between 1505 and 1945 the Dutch, Portuguese and English colonization had accelerated deforestation process in the Country (Mongabay, 2014). After independence timber production get increased, with the aim to fuel the economic and industrial development of the new nation. The government established ply-wood companies and other timber co-operations that heavily contributed to the continued deforestation through intensive logging, especially in the wet-zone. While the decades that followed, until today, witnessed a threefold population increase, the demand for Development project such as housing and commercial agricultural destroying the forest (Vitarana K.M, 1997).

Sri Lanka's natural forest cover has dwindled from 80% to less than 16% over the last 100 years. End of the 19th century, more than 80% of the country was covered by forest; at the beginning of the 20th century this rate had been reduced to 70 % and in 1950 only half of the land area was forested. In summary by the beginning of the 1990s forest cover remained less than a quarter of the country (Bogawattha, 1999). According to government, forest cover has shrunk back a further 5% over the 1990s (NPPD, 2002).

When we move into the 21st century, the threats to natural forest persist unabated and the national forest estate continues to be rapidly eroded. After 1970 huge development scheme called “the Mahaweli Irrigation Project” was implemented, with the main objective to irrigate large areas of the dry-zone in the northeast and make these soils more suitable for agriculture, especially for the production of rice. This project mainly implemented development in the jungle areas (Ranasingha D.M.S, 1998). Many development projects were accelerated deforestations in Sri Lanka and it has badly impact to reduce forest cover to 20% in 2007.

Following maps shows the deforestation from 1992 to 2007.

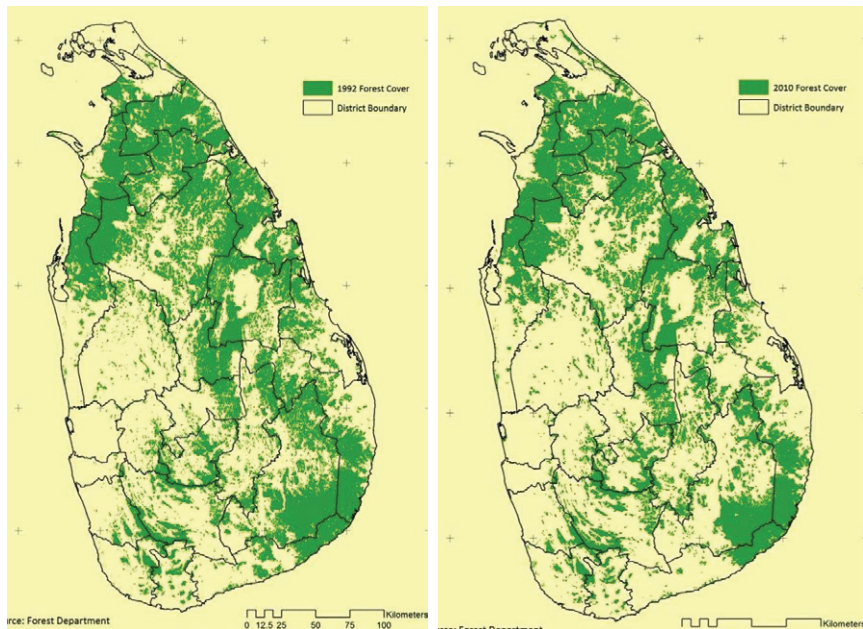


Figure 3: Changes of forest cover in Sri Lanka between 1992 and 2010 (REED+ Sri Lanka, 2007)

1.3. Remote Sensing applications in Forestry

Remote sensing is the acquisition of information about an object or phenomenon without making physical contact with the object and thus in contrast to on site observation. In modern usage, the term generally refers to the use of aerial sensor technologies to detect and classify objects on Earth (both on the surface, and in the atmosphere and oceans) by means of propagated signals (Wikipedia, 2017). Microwave Remote Sensing provides a unique opportunity to assess and monitor deforestation due its all-weather, day and night image acquisition capability unhindered by cloud cover; its potential to express surface roughness prominently; and its ability to penetrate the soil in certain cases.

1.4. Research problem

Sri Lanka is one of the few remaining countries in the world with extensive natural forest cover, but much of the existing forests have been destroyed, mainly by shifting cultivation, logging and by the growth of number of people involved in agriculture. Therefore the magnitude of deforestation and its consequences on natural processes need to be investigated. So an attempt was taken in this research to understand the changes in forest cover throughout the study area using remote sensing techniques.

1.5. Objectives

1.5.1. Main Objective:

Parameterizing the forest canopy using C- band SAR (Synthetic Aperture Radar) images.

1.5.2. Minor Objectives:

Detect the existing forest canopy using Space borne C band SAR images.

Detect forest canopy loss using Space borne C band SAR images.

1.6. Scope and limitations

The study area was selected as the Wilpattu in both Puttalam and Anuradhapura district because the area is highly deforested due to the human activities. Due to time limitation and also unavailability of free RADAR images, research was focused only for two data sets (2015 and 2016). Although there are many Earth observation techniques for deforestation analysis, Microwave Remote Sensing was used in this analysis. Freely available satellite images; Sentinel 1 C band SAR images were used for the study.

2. Literature Review

2.1. Microwave Remote Sensing for Forest Applications.

Microwave remote sensing has gained a lot of attention over the last decade with the availability of active radar imaging systems for a wide range of scientific applications. Especially SAR mounted on airborne or space borne platforms proved to be of great benefit due to their day and night capabilities and weather independence (<http://www.science.gov>, 02.03.2007). Few applications of radar remote sensing have been demonstrated towards the usefulness in the application of the forestry as the microwaves are capable of penetrating through the forest canopy and contribute to the monitoring of the forest and to understand the ecosystem processes. This ability of radar to penetrate the canopy and the expectation of retrieving biophysical forest descriptions has given a wide scope for forest radar research.

One research on “Mapping tropical forest cover and deforestation using (SAR) images” examines the capability of SAR data to assess and map deforestation. The results presented in this study suggest that dual polarization and quad-SAR data can suitably be used for the mapping of land covers and detects any changes. Forest can be separated reasonably well from other land covers and achieve accuracy more than 83% using SIR-C images (L- and C-bands, dual-polarizations).

2.1.1. Radar wavelength and polarization for forest applications

Depending on wavelength and polarization, radar can penetrate the canopy to different depths (figure 4), and can sense plant parts of different sizes, shapes, and water content. This ability of radar to probe the canopy, and the expectation of retrieving biophysical forest descriptions, underlie much of the international impetus for forest radar research (Sun et al, 1998).

Microwave interaction depends on the angle of incidence and wavelength of the Radar, dielectric properties and geometric arrangement of leafs and other canopy elements. X and C bands interact with the top part of the canopy layers. In P-band, the Radar waves can penetrate through the forest canopy, main branches, trunks and ground. L-band, the Radar waves penetrate through the primary, secondary branches, trunks and ground. It is illustrated that there exists the relationship between the C, L, P-band radar backscatter and forest biomass and growing stock volume (Tansey *et al* 2004). Hence, these bands are used to retrieve the canopy biophysical parameters.

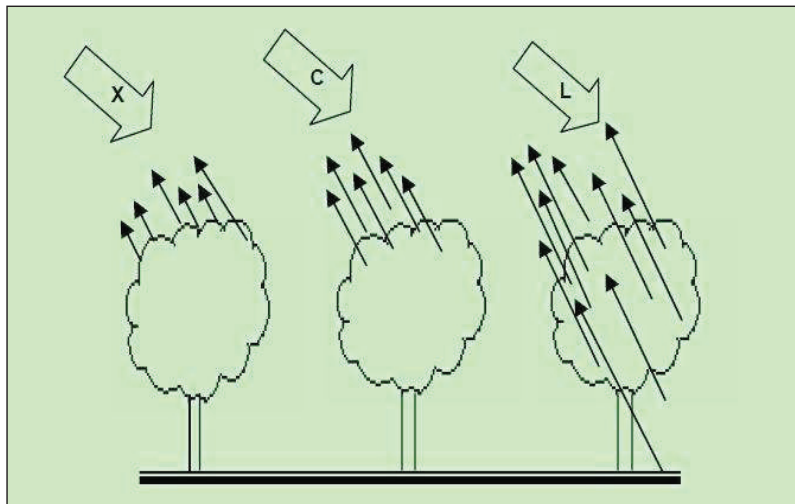


Figure 4: Penetration of different wave length in canopy (Vijayanthi N.V., 2008).

Trees and other vegetation are usually moderately rough on the longer wavelength scale. Hence, they appear as moderately bright features in the image. Structures of trees affect the backscattering coefficient (Touzi et al, 2004). Back scattering is the energy reflected from different earth surface objects, which is quite similar to the concept of spectral information in the optical imagery.

Backscattering and penetration varies within a forest canopy. In longer wavelengths, the effect of the trunk is very large. In shorter wavelengths, leaves play an important role in backscatter. This is due to the forest composition, tree density, and canopy thickness. The scattering properties are governed by size, shape and orientation of surface within forest canopy (Floyd et al, 1998). By visual interpretation, the different types of forests are discriminated using the backscatter intensity and texture. The parameters that are important in forest inventory are tree density, stand age and timber volume. These parameters are interrelated and also they depend on the tree growth and stand development.

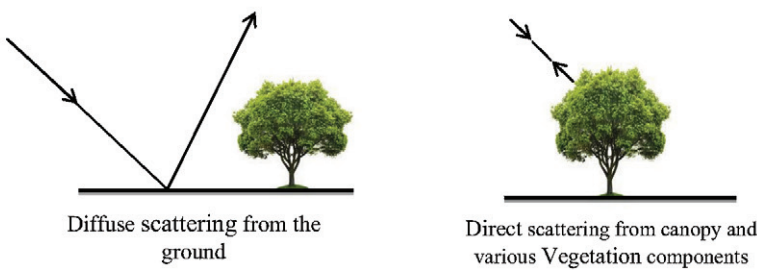
2.2. Scattering mechanism of forest

The total backscatter from forest land includes response from several components: crown volume scattering (dominant in C-band), backscattering from secondary branches and trunks (dominant in L-band), backscattering from ground, especially if canopy is sparse (for L-band) or

there is a gap in the canopy (both C- and L-bands), crown-ground (mostly in C-band) or trunk-ground (L-band) backscattering, often termed as double bounce (can be in both direction such as ground-trunk) (Rahman M.M.,2010). The magnitude of the scattering mechanisms and the importance of the different components are dependent on geometric factors (e.g., structural attributes of trees, canopy and soil surface roughness) and dielectric properties of vegetation and underlying surface (e.g., moisture content of vegetation and soil) (Dobson et al., 1995).

Structures of trees affect the backscattering coefficient (Touzi et al, 2004). Backscattering and penetration varies within a forest canopy. In longer wavelengths, the effect of the trunk is very large. In shorter wavelengths, leaves play an important role in backscatter. This is due to the forest composition, tree density, and canopy thickness. The scattering properties are governed by size, shape and orientation of surface within forest canopy (Floyd et al, 1998). By visual interpretation, the different types of forests are easily discriminated using the backscatter intensity and texture. The parameters that are important in forest inventory are tree density, stand age and timber volume. These parameters are interrelated and also they depend on the tree growth and stand development. Wavelength, polarization and incidence angle of radiation control these scattering mechanisms (Leckie and Ranson, 1998) and the final backscatter as a result of surface and/or volume scattering.

2.2.1. Scattering types in forests



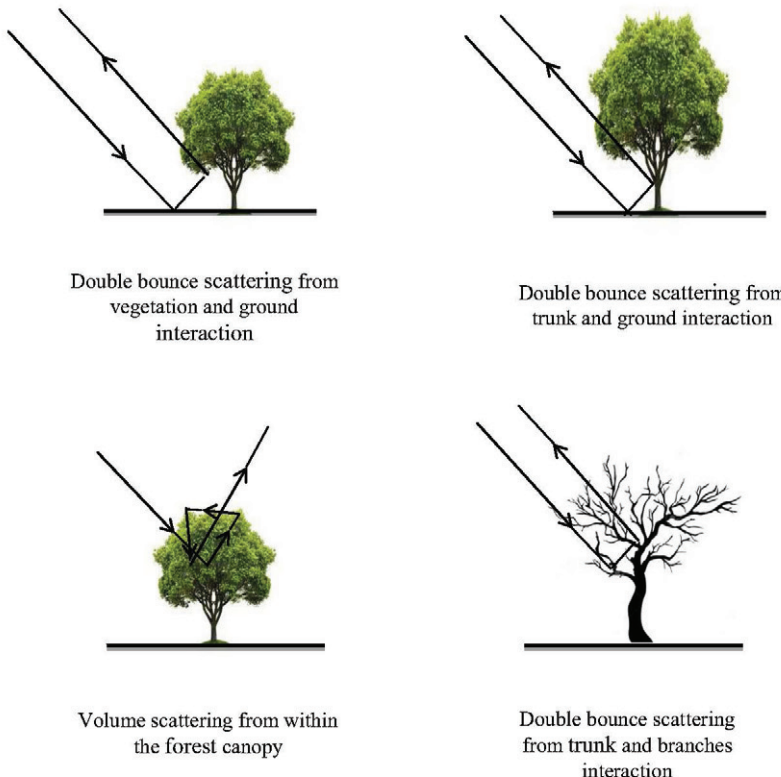


Figure 5: Scattering types in forests

The changes in tone and texture are related to crown closure or foliage density. Backscatter is dependent on crown closure than height (Floyd et al, 1998). Backscatter is also sensitive to the target's electrical properties, including water content.

The magnitude of the scattering mechanisms and the importance of the different components are dependent on geometric factors (e.g., structural attributes of trees, canopy and soil surface roughness) and dielectric properties of vegetation and underlying surface (e.g., moisture content of vegetation and soil) (Dobson et al., 1995). Wavelength, polarization and incidence angle of radiation control these scattering mechanisms (Leckie and Ranson, 1998) and the final backscatter as a result of surface and/or volume scattering.

2.3. Scattering mechanism in C band

2.3.1. C band SAR

A nominal frequency range, from 8 to 4 GHz (3.75 to 7.5 cm wavelength) within the microwave (RADAR) portion of the electromagnetic spectrum C-band has been the frequency of choice for several experimental aircraft SAR systems as well as a series of single-band satellite SAR systems, including the European ERS-1, ERS-2 and Envisat SAR systems and Canada's RADARSAT SAR. C-band is generally not hindered by atmospheric effects and is capable of 'seeing' through tropical clouds and rain showers. Its penetration capability with regard to vegetation canopies or soils is limited and is restricted to the top layers.

C band, which is an intermediate wavelength, with strong penetration of the radiation into the canopy enables further sources of scattering to be active and so there is some volume-scattering. Typical sources of scattering at C band are secondary branches and leaves (Ranson and Sun, 1994; Leckie and Ranson, 1998). The radar backscattering for SAR operating at shorter wavelengths such as C-band primarily occurs in the upper part of tree canopies and throughout most agricultural crops. SAR systems are sensitive to surface roughness (Harry Stern, 1998).

2.4. Change Detection using SAR data

In general, change detection involves the use of multi-temporal data sets to quantitatively analyse the temporal effects of the phenomenon (Lu et al., 2004). Digital change detection aims to detect changes over time. By and large the change detection system relies on differences in radiance value between two or more dates. There is no universally optimal technique; choice depends upon the application. Change map using post classification technique of two images will only be generally as accurate as the product of the accuracies of each individual classification. Review of change detection using multi-temporal remote sensing data has been carried out (Macleod and Congation, 1998; Mas, 1999; Lu, 2004; Jianya, 2008).

In order to extract the canopy changes in this study, the correlation coefficient, Coherence and the changes between pre-and post-event radar images are calculated for Wilpattu area. The reduction of the correlation coefficient is mainly expected from the deforested area with some radar illumination changes and temporal volume scattering changes but temporal behaviour of forest canopy and vegetation patches can be expected as the temporal difference of two images.

2.4.1. Complex Coherence Estimation

In SAR interferometry, coherence is defined as a measure of the degree of resemblance of RADAR phase between two SAR images of the same area and the degree of correlation that exists between the two SAR images is called the complex degree of coherence. Coherence provides a useful measure of the interferogram quality and the capability of applying efficiently phase unwrapping procedures (Rodriguez and Martin, 1992; Zebker et al., 1992). Coherence is obtained from the cross-product of the two registered Single Look Complex (SLC) images. The correlation between two complex signals S1 and S2 is generally expressed by the correlation coefficient (Eq. 2.1).

$$\gamma = \frac{\langle S_1 S_2^* \rangle}{\sqrt{\langle S_1 S_1^* \rangle \langle S_2 S_2^* \rangle}} \quad \dots \dots \dots \text{Equation 2.1}$$

Where, S1, S2 are complex values in SAR images and S* is the complex conjugate of S. the braces ($\langle \rangle$) indicate local spatial averaging around an individual multi-looked pixel (Bingyuan et al., 2008).

While the phase of γ corresponds to the effective phase difference the magnitude of γ describes the quality of the interferometric phase and ranges from zero (no correlation) to one (full correlation). It is affected by several factors as described by (Zebkeret et al., 1992a).

$$\gamma = \gamma_{tem} \gamma_{SNR} \gamma_{spec} \gamma_{vol} \quad \dots \dots \dots \text{Equation 2.2}$$

γ term denotes temporal correlation. Any change of the conditions between the two data acquisitions causes decorrelation. Several reasons can be noted, Man-made changes (e.g. agriculture, forestry)

1. Atmospheric effects
2. Changes of the dielectric properties of the backscatter due to moisture changes
3. Stochastic motion (e.g. tree leaves), the effects of which can be modeled (Zebkeret et al., 1992b).
4. Displacement of the surface in the size of one resolution cell or more leads to complete decorrelation.

Temporal decorrelation is the dominant factor in repeat pass interferometry. Its utilization for change detection targets predominantly man-made changes. Other factors of influence are negligible in comparison. γ_{SNR} is the decorrelation due to thermal noise. γ_{spec} is the spectral correlation. γ_{vol} describes the effect of volume backscattering. The Volume scattering plays a major role in forest applications. They create very high decorrelation in forest areas of SAR images. The calculated coherence is estimation from the data.

2.4.2. Image Differencing

In this method, two co-registered image dates are subtracted pixel by pixel in each band to produce a new change image between two dates (Singh, 1989; Jensen, 1996; Yuan et al.,).

$$I_d(x,y) = I_1(x,y) - I_2(x,y) \quad \dots \quad \text{Equation 2.3}$$

Where I_1 and I_2 are the images obtained from time1 and time 2, (x, y) are the coordinates of the pixels. The resulting image I_d represents the intensity difference of I_1 from I_2 . This technique works only if images are registered.

2.4.3. Image Rationing

Like the previous method, two co-registered image dates are rationed pixel by pixel in each band. The no-change area is characterized by ratio values close to 1 depending on the nature of changes between two dates changed areas will have higher or lower values (Singh, 1989).

$$I_r(x,y) = \frac{I_1(x,y)}{I_2(x,y)} \quad \dots \quad \text{Equation 2.4}$$

Where I_1 and I_2 are the images obtained from time1 and time 2, (x, y) are the coordinates of the pixels. The resulting image I_r represents the intensity ratio of I_1 from I_2 .

2.4.4. Correlation coefficient

$$\text{Correlation} = \frac{(I_1 - \mu_1) * (I_2 - \mu_2)}{\sigma_1 * \sigma_2} \quad \dots \dots \dots \text{Equation 2.5}$$

σ_1, σ_2 : Standard deviation of pixel values in image 1 and 2 respectively

μ_1, μ_2 : Mean of pixel values in image 1 and 2.

$\chi_{i,j}$: Correlation at i, j^{th} location

Pixel value on image 1 and 2 at i, j^{th} location

In theoretically, if any changes of geographical phenomena are occurred in between these two image acquisitions, the less correlation or minus relations are defining the change.

2.4.5. Texture Analysis

Texture is the pattern of intensity variations in an image and can be a valuable tool in improving land-cover classification accuracy. It contains important information about the structural arrangement of surfaces. The use of texture in addition to spectral features for image classification might be expected to result in some level of accuracy improvement, depending on the spatial resolution of the sensor and the size of the homogeneous area being classified (Coburn and Roberts, 2004; Ouma et al., 2006). The selection of suitable texture features is generally image as well as the feature of interest specific dependent. However, for some texture extraction approaches, the associated parameters can be determined through theoretical analysis while in other cases the texture features can only be extracted through trial-and-error methods (Mather M.P., 2011). Texture measures can produce new images by making use of spatial information inherent in the image. Mean and Standard Deviation Texture images were prepared in order to increase the classification accuracy of SAR images for detect the deforested areas.

A related research has been conducted in 2007. This study was covered Applications of image texture in forest classification (Kushwaha S. et al 2007). This research was mainly focused in classification of the forests which were affected by jhum (shifting cultivation) in north-eastern India. On this research the Large increases (11·1 %) in the classification accuracy were observed when texture and tone were used simultaneously. And the inverse difference moment was found to be more useful than the entropy.

Another related research on Texture analysis of SAR sea ice imagery using grey level co-occurrence matrices (Tsatsoulis C. et al 1999) was found that quantization, displacement, and orientation values that are the best for SAR sea ice texture analysis using GLCM.

2.4.5.1. Mean Texture

Mean can produce new images by making use of neighbouring pixels around the centre pixel of the window and centre pixel is replacing by Mean value.

$$\bar{x} = \frac{1}{m} \sum_{i=1}^m x_i \quad \dots \dots \dots \text{Equation 2.6}$$

x_i is the pixel values in the window

m is the number of pixels in the local window

2.4.5.2. Standard Deviation texture measure

STD produces new images by making use of neighbouring pixels around the center pixel of the window. And the center of the pixel window is replaced by calculated Standard Deviation for the window.

$$x = \frac{\sum_{i=1}^m (x_i - \bar{x})^2}{m - 1} \quad \dots \dots \dots \text{Equation 2.7}$$

x_i is the pixel values in the window

x is the pixel value for the centre pixel in the mean texture image

m is the number of pixels in the local window

\bar{x} is mean value in local window

2.4.5.3. Grey Level Co-occurrence Matrix

The principal concept of GLCM is that the texture information contained in an image is defined by the Contextual relationships that the grey tones in an image have to one another (Mather M.P., 2009). Texture information involves the information from neighbouring pixels which is important to characterize the identified objects or regions of interest in an image.

The Grey Level Co-occurrence Matrix (GLCM) proposed by Haralick R.M, 1973 is one of the most widely used methods to compute second order texture measures. Several texture features can be computed from the GLCM matrix, e.g., angular second moment, contrast, correlation, entropy, variance, inverse difference moment, difference average, difference variance, difference

entropy, sum average, sum variance and sum entropy (Haralick R.M., 1973). Each feature models different properties of the statistical relation of pixels co-occurrence estimated within a given moving window and along predefined directions and inter-pixel distances.

The GLCM is a measure of the probability of occurrence of two grey levels separated by a given distance in a given direction. The features can be categorized into three groups, i.e. contrast group, orderliness group and statistics group.

Contrast Group Features:

1. Contrast
2. Dissimilarity (DIS)
3. Homogeneity (HOM)

Orderliness Group Features:

4. Angular Second Moment (ASM)
5. Maximum Probability (MAX)
6. Entropy (ENT)

Statistics Group Features:

7. GLCM Mean
8. GLCM Variance
9. GLCM Correlation

3. Theoretical background

In this Section basic idea underlying the use of radar images, including radar fundamentals geometrical effects and the main factors affecting surface reflection or backscatter at radar wavelengths, are introduced and the discussion is based initially on the system components and functions of real aperture side-looking airborne radar (SLAR). The discussion then expands to include synthetic aperture radars (SAR) that have improved capabilities.

3.1. Remote Sensing

Remote sensing is the acquisition of data for deriving information about objects or materials (targets) located at the Earth's surface by using sensors mounted on platforms located at a distance from the targets. Here, measurements are made in different spectral regions on interactions between the targets and electromagnetic radiation (EMR). The field of remote sensing encompasses techniques that obtain precise information about earth's surface from a distance (Vijayanthi N.V., 2008). Remote sensing has proven to be an effective tool to monitor the land surfaces.

3.1.1. Remote sensing in forestry applications

Remote sensing offers significant features for forest management. Such as, the data can be acquired repeatedly (e.g. daily, monthly) that helps to monitor forest resources in a regular basis (Thejaswi G., 2007). These measurements can be made in near real time basis which is quite useful for monitoring events such as forest fire, remote sensing data has synoptic coverage and information can be acquired in places where accessibility is an issue, could use wavelengths that are not visible to human eye (Thejaswi G., 2007). Thus, remote sensing is the most effective means of assessing and monitoring forest resources. It is important to understand that remote sensing does not replace field survey but provides complimentary information (Thejaswi G., 2007). There are two types of remote sensing with respect to the type of energy resources, passive and active. And optical and microwave remote sensing with respect to the wave length region.

3.2. Classification of Remote Sensing systems according to the energy source

3.2.1. Passive systems

The sun provides a very convenient source of energy for remote sensing. The sun's energy is either reflected, as it is for visible wavelengths, or absorbed and then re-emitted, as it is for thermal infrared wavelengths.

Remote sensing systems which measure energy that is naturally available are called Passive Sensors they are detect the reflected or emitted electromagnetic radiation from natural sources. Examples for the passive systems are Microwave radiometer, magnetic sensor, cameras, optical mechanical scanner, spectrometer, microwave radiometer.

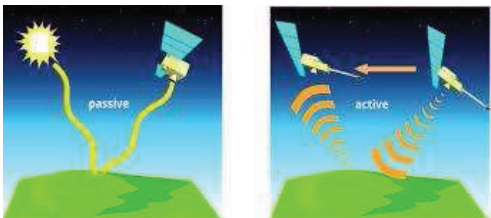


Figure 6: Active and Passive remote sensing systems

3.2.2. Active systems

Active systems provide their own energy source for illumination. The sensor emits artificially generated radiation which is directed toward the target to be investigated. The responses reflected from that object is detected and measured by the sensor. Advantages for active sensors include the ability to obtain measurements anytime, regardless of the time of day or season. Active sensors can be used for examining wavelengths that are not sufficiently provided by the sun, such as microwaves, or to better control the way a target is illuminated. Examples for the active systems are, microwave radiometer, microwave altimeter, laser, SONAR, Real Aperture Radar (RAR) and SAR (Mather M.P., 2009).

3.3. Classification of remote sensing systems with respect to the wave length

3.3.1. Optical remote sensing

The optical wavelength region (0.30-15.0 nm), an important region for remote sensing applications, is further subdivided as Visible (0.38-0.72nm), Near IR (0.72-1.30nm), Middle IR (1.30-3.00nm) and Far IR (7.00-15.0nm). The optical images with many visible and infrared channels were associated with specific applications because they are capable of providing fine spatial resolution and excellent multi spectral details, but they are inhabited by clouds and depend on solar illumination, and are thus limited to daylight observations. The limitation of clouds and darkness can be overcome by moving to the microwave portion of the spectrum

(Samuel W., 2009). Figure 7 which show only a part of the overall electromagnetic spectrum and it display the optical and microwave region of the spectrum.

3.3.2. Microwave Remote Sensing

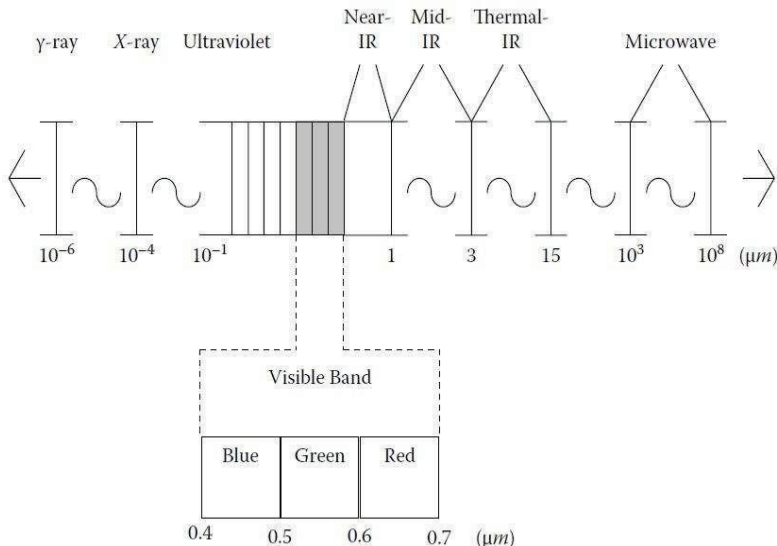


Figure 7: Regions of the electromagnetic spectrum that are of interest in remote sensing applications (Mather M.P., 2009).

Microwave remote sensing, using microwave radiation using wavelength from about one centimetre to few tens of centimetres enables observations in all weather conditions without any restrictions by cloud or rain (Dahdall B., 2011). There are two type of microwave remote sensing; active and passive. Active type receives the backscattering which is reflected from the transmitted microwave which is incidence on the ground surface and passive type receives the microwaves radiations emitted from objects on the ground. RADAR is an active microwave system which is used most of the cases in remote sensing.

3.4. RADAR remote sensing for forest applications.

Microwave remote sensing is very useful in the application of the forestry as the microwaves are capable of penetrating through the forest canopy and contribute to the monitoring of the forest and to understand the ecosystem processes. It provides continuous observation of the earth's surface regardless of the atmospheric conditions (Kasischke et al., 1997). The all-weather

capability, signal independence to the solar illumination angle and response to 3D vegetation structures are the highlights of active radar systems for natural vegetation mapping and monitoring.

Radar remote sensing is also used to achieve biomass estimates and carbon accounting. Radar data can also provide information about terrain surface and vegetation canopies (Heri et al, 1999). SAR provides important characteristics of soil and vegetation covers for instance, inundation below closed canopies, fresh woody biomass of forested areas, freeze/thaw conditions of soil and vegetation, soil moisture and surface roughness in areas of low vegetation, and information on the orientation and structure of objects on the ground that reflect the incoming microwave radiation. These capabilities provide enormous potential for data fusion between SAR and optical sensors to improve capability of performing global remote sensing of changes in land cover and land use. SAR sensors have promises to significantly enhance the capabilities to map land cover and land use as they operate with multiple polarizations and large swath widths. SAR provides its own illumination at frequencies that can penetrate clouds and smoke to provide information at high spatial and temporal resolution within and below the canopy (Kasischke et al., 1997).

3.5. RADAR

The word radar is an acronym derived from the phrase “Radio Detection And Ranging.” Imaging microwave sensors are known as imaging radars. These instruments transmit a signal in the frequency of 0.3 GHz to 300 GHz, or wavelength range approximately 3 cm to 1 m, and receive reflection (backscatter) from the target (Mather M.P., 2009). Remote sensing in the microwave region differs from optical remote sensing in a number of ways, the most important of which are,

1. Radar backscatter is related to the roughness and electrical conductivity of the target. This information is complementary to that which is acquired by optical and thermal sensors (Mather M.P., 2009).
2. Microwave imaging radars are active, not passive instruments, and thus can operate independently of solar illumination (Mather M.P., 2009).
3. Energy in the microwave region can penetrate clouds thus Microwave enables observations in all weather conditions without any restrictions by cloud or rain.

Imaging radar is classified further into RAR and SAR.

3.5.1. Real Aperture Side-looking Airborne Radar (SLAR).

RAR is a form of radar that transmits a narrow angle beam of pulse radio wave in the range direction at right angles to the flight direction and receives the backscattering from the targets which will be transformed to a radar image from the received signals. Usually the reflected pulse will be arranged in the order of return time from the targets, which corresponds to the range direction scanning. The resolution in the range direction depends on the pulse width. The resolution in the azimuth direction is identical to the multiplication of beam width and the distance to a target (Mather M.P., 2009).

3.5.2. Synthetic Aperture Radar (SAR)

Synthetic-aperture radar (SAR) is a form of radar which moves a real aperture or antenna through a series of positions along the objects to provide distinctive long-term coherent-signal variations. In contrast to real aperture radar systems, SAR makes use of the Doppler effect of the motion of platforms (satellite or aircraft) to increase the “aperture” and thus the resolution of the images.

3.5.3. Basic principle of RADAR

The basic principle of Radar is to send out a signal and measure the time taken until it returns to

the source, thus measuring the distance to that target.

The principle of Radar working is shown in figure 8
The transmitter generates successive pulses of microwave (A) at regular intervals which are focused by the antenna into a beam (B). The radar beam illuminates the surface obliquely at a right angle to the motion of the platform. The antenna receives a

portion of the transmitted energy reflected from various objects within the illuminated beam (C). By

measuring the time delay between the transmission of a pulse and the reception of the backscattered "echo" from different targets, their distance from the radar and thus their location can be determined. As the sensor platform moves forward, recording and processing of the backscattered signals builds up a two-dimensional image of the surface (Vyjayanthi N. dt al 2008).

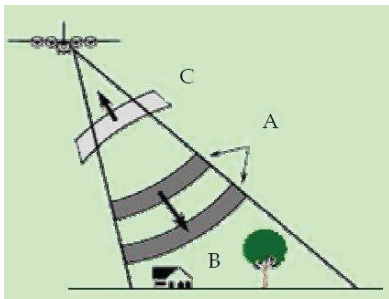


Figure 8: Radar working principle

3.5.4. RADAR image geometry

SAR data acquires an image in each pixel record both the amplitude and phase of the back-scattered signals from the resolution cell using a complex number.

$$\text{complex signal} = A \cos \varphi + A \sin \varphi \quad \dots \quad \text{Equation 3.1}$$

Where, $A = \text{Amplitude}$

$\varphi = \text{Phase}$

This is a complex image. In this image brighter areas represent high backscatter, darker areas represents low backscatter the level of backscatter for each pixel over the imaged area is depending upon the backscatter from the ground. This complex digital number can be used to find both intensity and phase band.

3.5.4.1. Intensity

Intensity of a RADAR image measures the strength of the backscattered signal and it is directly related to the both Radar system properties such as wavelength (frequency) of radar, incidence angle, polarization, viewing geometry and target parameters such as surface roughness, dielectric properties, Thickness or volume of surface cover, Surface Geometry. Intensity is computed by,

$$\text{Intensity} = \sqrt{I^2 + Q^2} \quad \dots \quad \text{Equation 3.2}$$

Where, $Q = A \sin \varphi$

$I = A \cos \varphi$

$A = \text{Amplitude}, \varphi = \text{phase}$

3.5.4.2. Phase

The most important parameter that a SAR measures is phase, which equals twice the range R to the scattering centre of each pixel with 2π radian period, divided by the radar wavelength λ and is computed by,

$$\text{Phase } (\varphi) = \arctan \left(\frac{Q}{I} \right) \quad \dots \quad \text{Equation 3.3}$$

$$\text{Phase of RADAR image} = \frac{4\pi R}{\lambda} \quad \dots \quad \text{Equation 3.4}$$

Where $Q = A \sin \varphi$

$$I = A \cos \varphi$$

A = Amplitude

φ = phase

The phase of a SAR image is actually the phase difference between the backscattered signal and the reference signal (Dahdal B., 2011). The phase of the return wave depends on the distance to the ground, since the path length to the ground and back will consist of a number of wavelengths plus some fraction of a wavelength. This is observable as a phase difference or phase shift in the returning wave. The total distance to the satellite (or the number of whole wavelengths) is not known, but the extra fraction of a wavelength can be measured extremely accurately (Massonnet and Feigl, 1998).

3.5.5. RADAR Image Resolutions

Imaging geometry of radar system is different from the scanning systems commonly used in optical remote sensing. The azimuth resolution and the slant-range resolution govern the resolution of RADAR (Mather M.P., 2009). Range refers across-track dimension perpendicular to the flight direction, while azimuth refers along-track dimension parallel to the flight direction.

3.5.5.1. Azimuth Resolution

RADAR terminology, the width of ground area illuminated by each pulse of electromagnetic radiation is called as Azimuth resolution. The azimuth increases with increasing distance from the radar.

$$\text{Azimuth Resolution} = \beta * d \quad \dots \quad \text{Equation 3.5}$$

$$\text{Azimuth Resolution} = \beta = \frac{\lambda}{L} \quad \dots \quad \text{Equation 3.6}$$

By Equation 3.1 and Equation 3.2,

$$\text{Azimuth Resolution} = \frac{\lambda}{L} * d \quad \dots \quad \text{Equation 3.7}$$

Where,

β is the antenna beam width.

d is the ground range.

λ is the wave length

L is the antenna length

According to Eq. (3.7), one can use a long antenna length and short wavelength to obtain finer azimuth resolution. However, shorter wavelengths are more likely to be affected by the atmosphere and, furthermore, antenna length is constrained by physical limitations (Mather M., 2009). An alternative strategy is used to obtain a finer resolution for azimuth is known as synthetic aperture radar (SAR).

3.5.5.2. Range Resolution

Range is the direction perpendicular to flight path of the aircraft and the range resolution of the RADAR system is its ability to distinguish two objects separated by some minimum distance (Samuel W., 2007). The slant range resolution is computed by,

$$\frac{\text{Slant range}}{\text{resolution}} = \frac{c\tau}{2} \quad \dots \quad \text{Equation 3.8}$$

Ground range, in which distances are measured between the platform ground track and the target, then

$$\frac{\text{Ground range}}{\text{resolution}} = \frac{c\tau}{2 \sin \theta} \quad \dots \quad \text{Equation 3.9}$$

C is the velocity of light ($3 \times 10^8 \text{ ms}^{-1}$).

τ is Pulse duration.

θ is incidence angle of the RADAR beam.

It can be concluded from Equation (3.9) that the shorter the pulse duration τ , or the larger the value of, θ the finer the range resolution. The incidence angle θ varies across an image. The value of θ in the near range is relatively smaller than that in the far range. Thus, the ground range resolution will also vary with respect to θ that is far ground range resolution has a higher resolution than that in near ground range (Mather M.P., 2009).

3.5.6. RADAR viewing Geometry

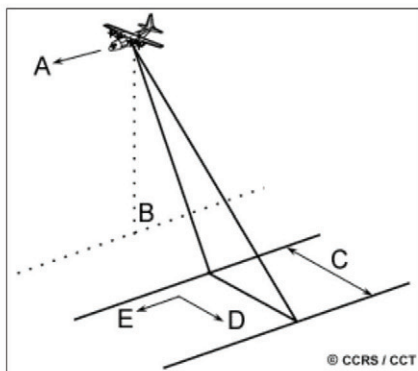


Figure 9: RADAR viewing geometry

(<http://www.nrcan.gc.ca>, 2017).

the across-track dimension perpendicular to the flight direction, while azimuth (E) refers to the along-track dimension parallel to the flight direction. This side-looking viewing geometry is typical of imaging radar systems (airborne or space borne) and it associate with number of terms which are describes in below.

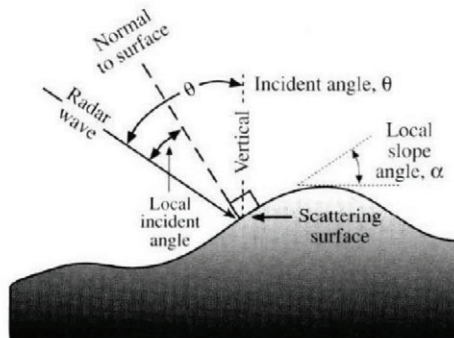


Figure 10: The relationship between radar incident angle (θ) true vertical and local slope angle (α) for non-level terrain

(<http://www.nrcan.gc.ca>, 2017)

is no relationship between depression angle and incident angle. The incident angle best describes the relationship between the radar beam and surface slope. A schematic diagram of the relationship is shown in Figure 10. Many mathematical radar studies assume the terrain surface

The imaging geometry of a radar system (Figure 9) is different from the framing and scanning systems commonly employed for optical remote sensing. Similar to optical systems, the platform travels forward in the flight direction (A) with the nadir (B) directly beneath the platform. The microwave beam is transmitted obliquely at right angles to the direction of flight illuminating a swath (C) which is offset from nadir. Range (D) refers to

3.5.6.1. Incidence angle (θ)

The incident angle θ is the angle between the radar pulse of electromagnetic energy and a line perpendicular to the Earth's surface where it makes interaction.

When the terrain is flat, the incident angle of the radar beam is the complement of the depression angle. However, if the terrain is sloped, there

is flat (horizontal) therefore, the incident angle is assumed to be the complement of the depression angle.

3.5.6.2. Look angle

The look angle is the angle at which the radar "looks" at the earth surface. In the near range, the viewing geometry may be stated to as being steep, relative to the far range, where the viewing geometry is shallow.

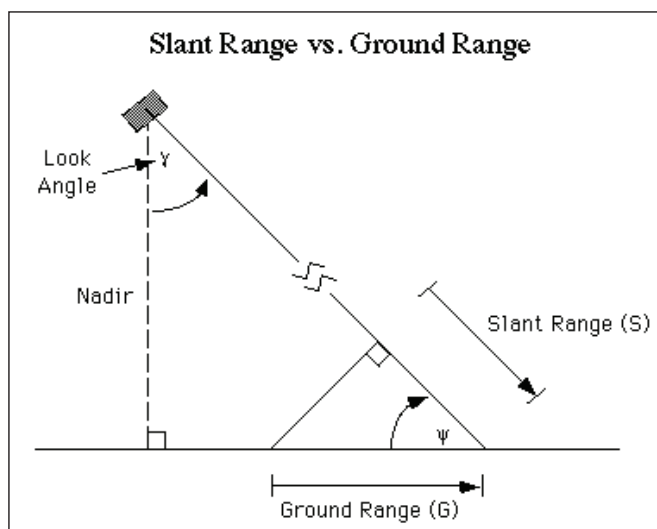
3.5.6.3. Near Range and Far Range

The portion of the image swath closest to the nadir track of the radar platform is known as the near range while the portion of the swath farthest from the nadir is known as the far range.

3.5.6.4. Slant Range and Ground range

At all ranges the radar antenna measures the radial line of sight distance between the radar and each target on the surface. This is known as the slant range distance.

The ground range distance is the true horizontal distance along the ground to each point



measured in slant range. The viewing geometry of a radar results in certain geometric distortions on the resultant imagery (Stamondo S. and Montouori A., 2011).

Figure 11: Slant range and Ground range of RADAR system

(<http://www.nrcan.gc.ca>, 2017).

3.5.7. Geometric distortions on RADAR images

As with all remote sensing systems, the viewing geometry of a radar results in certain geometric distortions on the resultant imagery such as scale distortions, foreshortening, layover and shadow. However, there are key differences for radar imagery which are due to the side-looking viewing geometry, and the fact that the radar is fundamentally a distance measuring device (i.e. measuring range).

3.5.7.1. Scale distortions

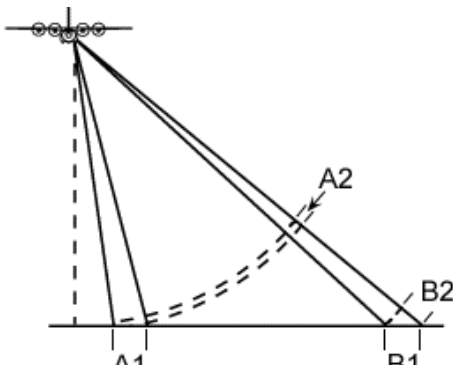


Figure 12: Slant range scale distortion
(<http://www.nrcan.gc.ca>, 2017).

Slant range scale distortion occurs because the radar is measuring the distance to features in slant-range rather than the true horizontal distance along the ground. This results in a varying image scale, moving from near to far range. Although targets A1 and B1 are the same size on the ground, their apparent dimensions in slant range (A2 and B2) are different. This causes targets in the near range to appear compressed relative to the far range. Using trigonometry, ground-range distance can be calculated from the slant-range distance and platform altitude to convert to the proper ground-range format (Stamondo S. and Montouori A., 2011).

3.5.7.2. Relief Displacement

Tall objects on Earth surface are displaced radially from nadir due to side looking geometry of the RADAR system this is known as relief displacement which is directly proportional to the height of the vertical structure and increases when the structure is closer to the nadir.

$$\text{Relief displacement in slant range} \approx h \sin\theta \quad \dots \quad \text{Equation 3.10}$$

$$\text{Relief displacement in ground range} \approx h \tan\theta \quad \dots \quad \text{Equation 3.11}$$

Where h is the height of the object θ is incidence angle of the RADAR beam

3.5.7.3. Layover

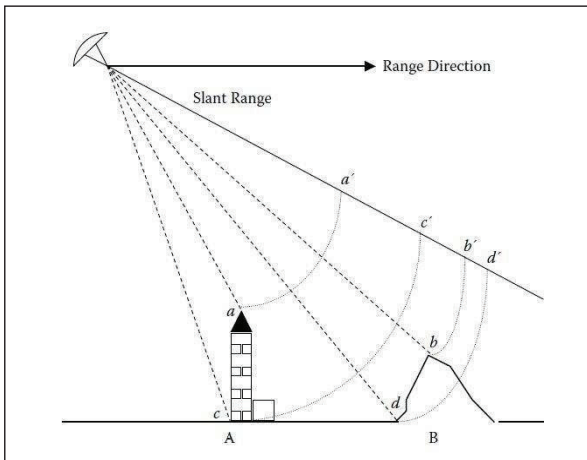


Figure 13: Layover effect on RADAR images (Mather M.P., 2009).

The layover effect results when the top of an illuminated target is seen by the radar as the bottom, and the bottom of the target is recorded by radar as the top (Mather M.P., 2009). In the case of a very steep slope, targets in the valley have a larger slant range than related mountain tops thus reflected energy from the

upper portion of a feature is received before the return from the lower portion then the fore slope is "reversed" in the slant range image. Figure 13 shows two targets (a building and a mountain) that are illuminated by a radar sensor. The microwave energy transmitted by the radar will reach the tops of both objects (points a and b in Figure 13) before the bottoms (points c and d). The antenna will first receive the reflected energy from a and b, then some time later, the energy reflected from c and d. After projection onto the slant range domain, the result is called the layover effect (Mather M.P., 2009).

3.5.7.4. Fore shortening

Foreshortening in a radar image is the appearance of compression of those features in the scene which are tilted toward the radar. Foreshortening leads to relatively brighter appearance of these slopes, and must be accounted for by the interpreter.

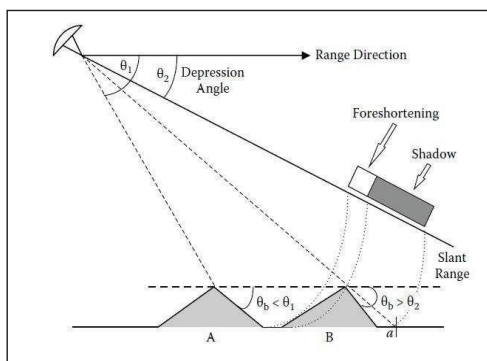


Figure 14: foreshortening and shadow in RADAR images (Mather M.P., 2009).

Foreshortening is at a maximum when a steep slope is orthogonal to the radar beam. In this case, the local incident angle is zero, and as a result, the base, slope and top of a hill are imaged simultaneously and, therefore, occupy the same position in the image (<http://www.nrcan.gc.ca>, 2017).

3.5.7.5. Shadow

Radar shadow is due to the returned back energy from targets being affected by the nature of the terrain (Mather M.P., 2009). Closer objects have less potential shadowing than farther objects and Shadows only occur in cross-track or in down-range direction behind tall objects and a good indicator of radar illumination direction. Since incident angle increases from near to far-range shadowing becomes more prominent toward far range. Radar shadows contain information about the system noise and the object height.

The type and degree of relief displacement in the radar image is a function of the angle at which the radar beam hits the ground, i.e. it depends upon the local slope of the ground.

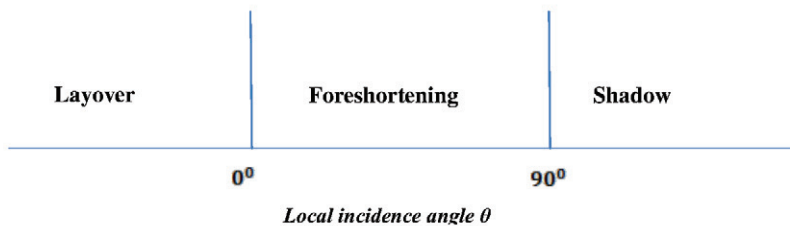


Figure 15: Relationship between Geometric distortions and incidence

3.5.7.6. Speckles

Due to random fluctuations in the signal observed from a spatially extensive target represented by a pixel (or image resolution element), speckle noise is generally present on a radar image. Speckle has the characteristics of a random multiplicative noise in the sense that as the average grey level of a local area increases, the noise level increases. In a SAR imaging system, speckle effects are more serious (Lopez M. and Fabregas, 2003).

There are two approaches to the suppression of radar image speckle. The first method is known as the multilook process, while the second method uses filtering techniques to suppress the speckle noise (Mather M.P., 2009).

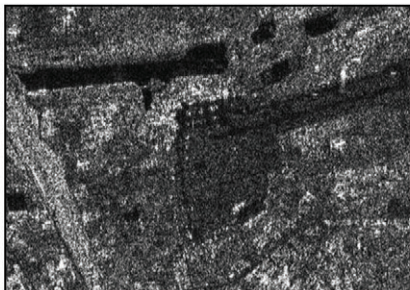


Figure 17: RADAR image with speckles (Mather M.P., 2009).



Figure 17: RADAR image without speckles (Mather M.P., 2009).

3.5.8. RADAR Waveform Properties

An active radar system repetitively transmits short microwave energy pulses (normally of the order of microseconds, i.e., 10–6 second, denoted by μ s) toward the area to be imaged (Mather M.P., 2009). Each energy pulse has duration of between 10 and 50 μ s, and utilizes a small range of microwave wavelengths. A waveform can be characterized in terms of its wavelength, amplitude, frequency and polarization.

3.5.8.1. Wavelength and Frequency

Wavelength is defined as the distance between two adjacent crests or troughs of the waves (Figure 18) (Mather M.P., 2009). Radar Systems are able to measure the following wave length bands (Table 1) each of the band is specific for the different radar applications,

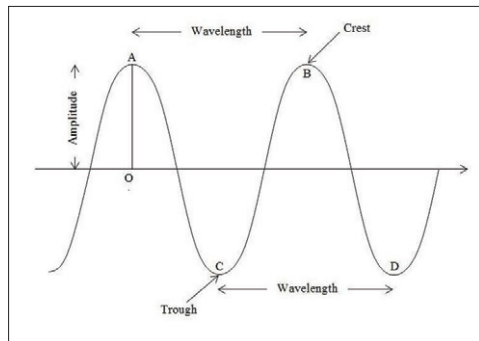
Table 1 Radar frequency and wave length

Band	Frequency (GHz)	Wave length(cm)
P band	0.3-1	30-100
L band	1-2	15-30
S band	2-4	7.5-15
C band	4-8	3.76-7.5
X band	8-12.5	2.4-3.75
u band	12.5-18	1.67-2.4
K band	18 -26.5	1.1-1.67
Ka band	26.5 - 40	0.75-1.1

Source: Radar basics -Part 1, Parker M.

3.5.8.2. Amplitude

Amplitude measures the strength of an electromagnetic wave in terms of the maximum distance achieved by the waveform relative to the mean position (shown by the horizontal line in Figure 18). The amplitude may be a function of a complex signal including both magnitude and the phase (Mather M.P., 2009).



3.5.8.3. Polarization

Polarization is an important property of a plane EM wave. Polarization refers to the alignment and regularity of the Electric and Magnetic Field components of the wave, in a plane perpendicular to the direction of propagation (<http://www.nrcan.gc.ca>, 2017).

The two most common basis polarizations in RADAR systems are horizontal linear or H, and vertical linear or V. Circular polarizations are also in use for some applications, e.g. weather radars.

A radar system using H and V linear polarizations can thus have the following channels:

- HH - for horizontal transmit and horizontal receive, (HH)
- VV - for vertical transmit and vertical receive, (VV)
- HV - for horizontal transmit and vertical receive (HV), and
- VH - for vertical transmit and horizontal receive (VH).

The RADAR systems are capable to measure more than one polarization at a single time. These phases play an important role in polarimetric information extraction.

3.5.9. RADAR equation

The radar principle is based on the properties of electromagnetic waves and its characteristic reflection at different objects on Earth surface. Thereby, a RADAR microwave signal of wavelength λ is transmitted. Based on the reflected and received signal response conclusions regarding direction, distance, and relative velocity of the reflecting target can be drawn. The

received signal strength of the target can be calculated after the radar equation (Van Zyl et al., 1993).

The parameters of the radar equation (Van Zyl et al., 1993) are fundamental factors that influence the level of the returned signal. The radar equation is expressed as,

$$P_r = \frac{P_t \lambda G_t(\gamma) G_r(\gamma)}{(4\pi)^3 R^4} \sigma^o A \quad \dots \dots \dots \text{Equation 3.6}$$

P_t is the transmitted power from the antenna

λ is the transmitted wavelength

R is the distance to imaging area

γ is the radar look angle

A is the area on the ground responsible for scattering

G_t and G_r are the transmitted and received antenna gains

(Describing the system's ability to focus the transmitted microwave energy) at look angle

γ

σ^o is the radar backscatter coefficient measured

3.5.10. RADAR Backscatter

Backscatter is the portion of the outgoing radar signal that the target redirects directly back towards the radar antenna. Backscattering is the process by which backscatter is formed. The scattering cross section in the direction toward the radar is called the backscattering cross section; the usual notation is the symbol sigma (σ). It is a measure of the reflective strength of a radar target. The normalized measure of the radar return from a distributed target is called the backscatter coefficient, or sigma naught (σ^o), and is defined as per unit area on the ground. If the signal formed by backscatter is undesired, it is called clutter. Other portions of the incident radar energy may be reflected and scattered away from the radar or absorbed.

4. Study area and Data

4.1. Study Area

This study was attempt to Wilpattu national park (8.4106° N, 80.0511° E) has the most intense recent large-scale forest clearance which is located in the Northwest coast lowland dry zone in Sri Lanka. The park is located 30 km west Anuradhapura and located 26 km north of Puttalam (approximately 180 km north of Colombo). The park is 131, 693 hectares and ranges from 0 to 152 meters above sea level. Nearly sixty lakes (Willu) and tanks are found spread throughout Wilpattu.

Wilpattu is the largest and one of the oldest National Parks in Sri Lanka. Wilpattu is among the top national parks world-renowned for its leopard (*Panthera pardus kotiya*) population (https://en.wikipedia.org/wiki/Wilpattu_National_Park, 17.05.2017).

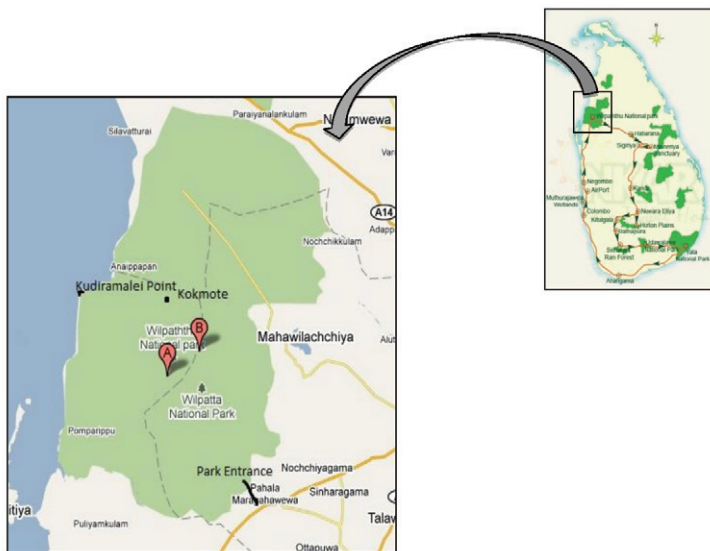


Figure 19: Location of Wilpattu National Park (Not to Scale)

4.2. Data

Sentinel 1 Single-Look Complex (SLC) imagery data have been selected for this study. The frequency band used in the study is C-band (4-8 GHz/ 3.75 cm to 7.5 cm). The following rephrases are describes a brief overview about Sentinel 1 Mission and the Sentinel 1 Data. The following discussion is completely based on the Sentinel 1 User Hand Book

4.2.1. Sentinel I Mission

SENTINEL-1 continues the C-band SAR Earth Observation of ESA's ERS-1, ERS-2 and ENVISAT, and Canada's RADARSAT-1 and RADARSAT-2. The SENTINEL-1 mission is the European Radar Observatory for the Copernicus joint initiative of the European Commission (EC) and the European Space Agency (ESA) (<https://sentinel.esa.int/>, 12.05.2017).

SENTINEL-1 is an imaging radar mission providing continuous all-weather, day-and-night imagery at C-band (Rahman M.M., 2010). The SENTINEL-1 constellation provides high reliability, improved revisit time, geographical coverage and rapid data dissemination to support operational applications in the priority areas of marine monitoring, land monitoring and emergency services (Rahman M.M., 2010). It includes four exclusive imaging modes with different resolution (down to 5 m) and coverage (up to 400 km) and provides dual polarization capability, very short revisit times and rapid product delivery.

SENTINEL-1 will be in a near-polar, sun-synchronous orbit with a 12 day repeat cycle and 175 orbits per cycle for a single satellite. Both SENTINEL-1A and SENTINEL-1B share the same orbit plane with a 180° orbital phasing difference. With both satellites operating, the repeat cycle is 6 days.

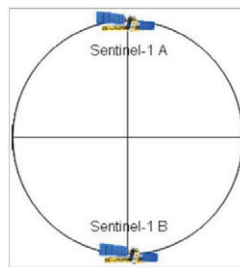


Figure 20: SENTINEL-1 Constellation

4.2.2. SENTINEL-1 operating modes

SENTINEL-1 operates in four exclusive acquisition modes Stripmap (SM), Interferometric Wide swath (IW), Extra-Wide swath (EW), and Wave mode (WV).

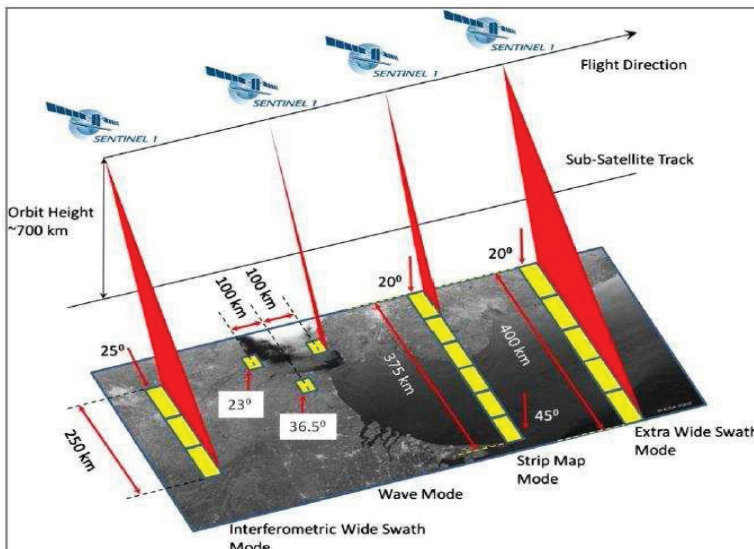


Figure 21: SENTINEL-1 Operating Modes (<https://sentinel.esa.int/>, 12.05.2017).

Stripmap Mode

Stripmap imaging mode is provided for continuity with ERS and ENVISAT missions. Stripmap provides coverage with a 5 m by 5 m resolution over a narrow swath width of 80 km. One of six imaging swaths can be selected by changing the beam incidence angle and the elevation beam width (<https://sentinel.esa.int/>, 12.05.2017).

Interferometric Wide Swath Mode

The Interferometric Wide swath (IW) mode allows combining a large swath width (250 km) with a moderate geometric resolution (5 m by 20 m). The IW mode images three sub-swaths using Terrain Observation with Progressive Scans SAR (TOPSAR). The TOPSAR technique ensures homogeneous image quality throughout the swath. The IW mode is the default acquisition mode over land (<https://sentinel.esa.int/>, 12.05.2017).

Extra Wide Swath Mode

The Extra Wide swath imaging mode is intended for maritime, ice and polar zone operational services where wide coverage and short revisit times are demanded. The EW mode works similarly to the IW mode employing a TOPSAR technique using five sub-swaths instead of three, resulting in a lower resolution (20 m by 40 m). The EW mode can also be used for interferometry as with the IW mode (<https://sentinel.esa.int/>, 12.05.2017).

Wave Mode

SENTINEL-1 Wave mode, in conjunction with global ocean wave models, can help determine the direction, wavelength and heights of waves on the open oceans. Wave mode acquisitions are composed of Stripmap images of 20 km by 20 km, acquired alternately on two different incidence angles (<https://sentinel.esa.int/>, 12.05.2017).

4.2.3. Sentinel 1 data products

SENTINEL data products are made available systematically and free of charge to all data users including the general public, scientific and commercial users. All data products are distributed in the SENTINEL Standard Archive Format for Europe (SAFE) format.

Each mode can potentially produce products at SAR Level-0, Level-1 SLC, Level-1 GRD, and Level-2 OCN.

Data products are available in single polarizations (VV or HH) for Wave mode and dual polarizations (VV+VH or HH+HV) and single polarization (HH or VV) for SM, IW and EW modes.

Level-0

The SAR Level-0 products consist of the sequence of Flexible Dynamic Block Adaptive Quantization (FDBAQ) compressed unfocused SAR raw data. For the data to be usable, it will need to be decompressed and processed using focusing software.

Level-1

Level-1 data are the generally available products intended for most data users. Level-1 products are produced as Single Look Complex (SLC) and Ground Range Detected (GRD).

1. **Level-1 Single Look Complex (SLC)** products consist of focused SAR data geo-referenced using orbit and attitude data from the satellite and provided in zero-Doppler slant-range geometry. The products include a single look in each dimension using the full TX signal bandwidth and consist of complex samples preserving the phase information.
2. **Level-1 Ground Range Detected (GRD)** products consist of focused SAR data that has been detected, multi-looked and projected to ground range using an Earth ellipsoid model. Phase information is lost. The resulting product has approximately square resolution pixels and square pixel spacing with reduced speckle at the cost of reduced geometric resolution.

Level-2

Level-2 OCN products include components for Ocean Swell spectra (OSW) providing continuity with ERS and ASAR WV and two new components: Ocean Wind Fields (OWI) and Surface Radial Velocities (RVL) (<https://sentinel.esa.int/>, 12.05.2017).

4.2.4. Description about used Data

Table 2: Selected Sentinel 1 Data

No	Acquisition Date	Mode	Product Type	Polarization
1	2015.06.04	IW (Interferometric Wide Swath)	SLC (Single Look Complex Data)	VV Polarization (Single Polarization)
2	2015.08.15			
3	2015.11.19			
4	2016.01.06			
5	2016.07.16			
6	2016.08.09			
7	2016.03.18			
8	2016.09.26			VV+VH Dual Polarization

4.2.5. Auxiliary Data Sets

SRTM 90m DEM has been used to co-register and geocode the temporal images.

4.2.6. Tools Used

For image processing SNAP tool box develop by European space agency. ENVI 5.0 and MATLAB used for further processing of SAR images and ARC map for design the output map and finally Microsoft Excel was used for analyse the results statically.

5. Methodology

5.1. Acquiring Sentinel 1 (SLC) data

Sentinel 1 Single-Look Complex (SLC) imagery data have been selected for this study. Descriptions about selected data were mentioned on previous chapter 4. All the satellite images were downloaded through the Scientific Hub (<https://scihub.copernicus.eu/dhus/#/home>,

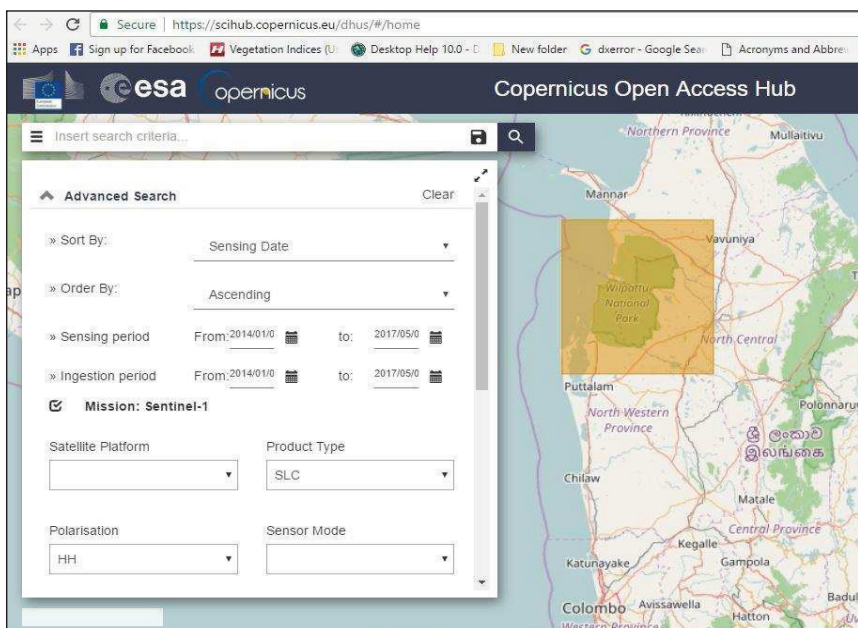


Figure 22: Scientific Hub selection window

12.12.2016). After selecting the satellite platform, Product type, polarization, sensor mode and other relevant searching criteria's the system displaying available datasets for the required area. Then user can download the data for their applications without any cost.

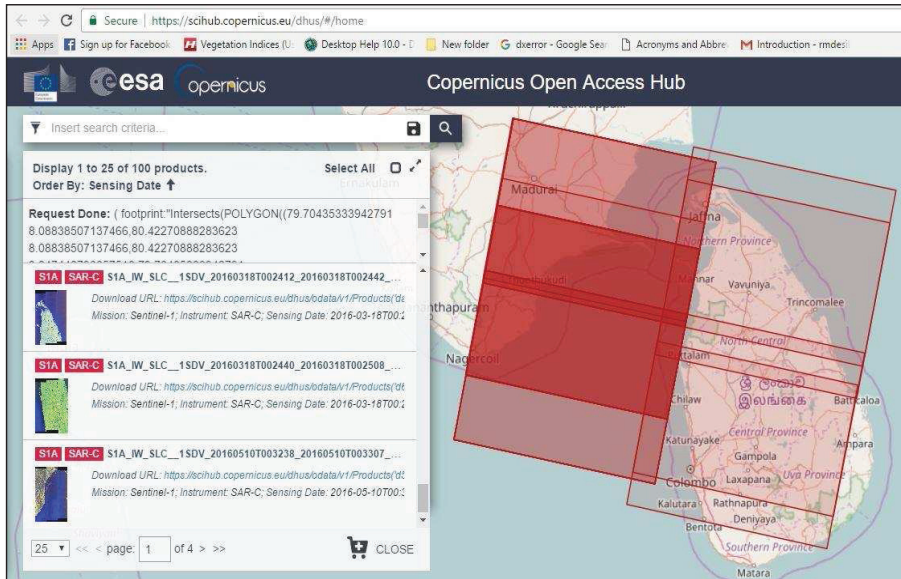


Figure 23: Displayed data sets for selected area.

After downloading the data, the imageries have been corrected for several atmospheric and sensor distortions before they used for applying specific change detection and analysis techniques. The following rephrases about RADAR pre-processing was based on the User guide of the SNAP Platform.

After downloading the necessary data the overall framework involved in the study for accomplishing its objective is as follows (figure 24).

5.2. The flow chart of the methodology of this study

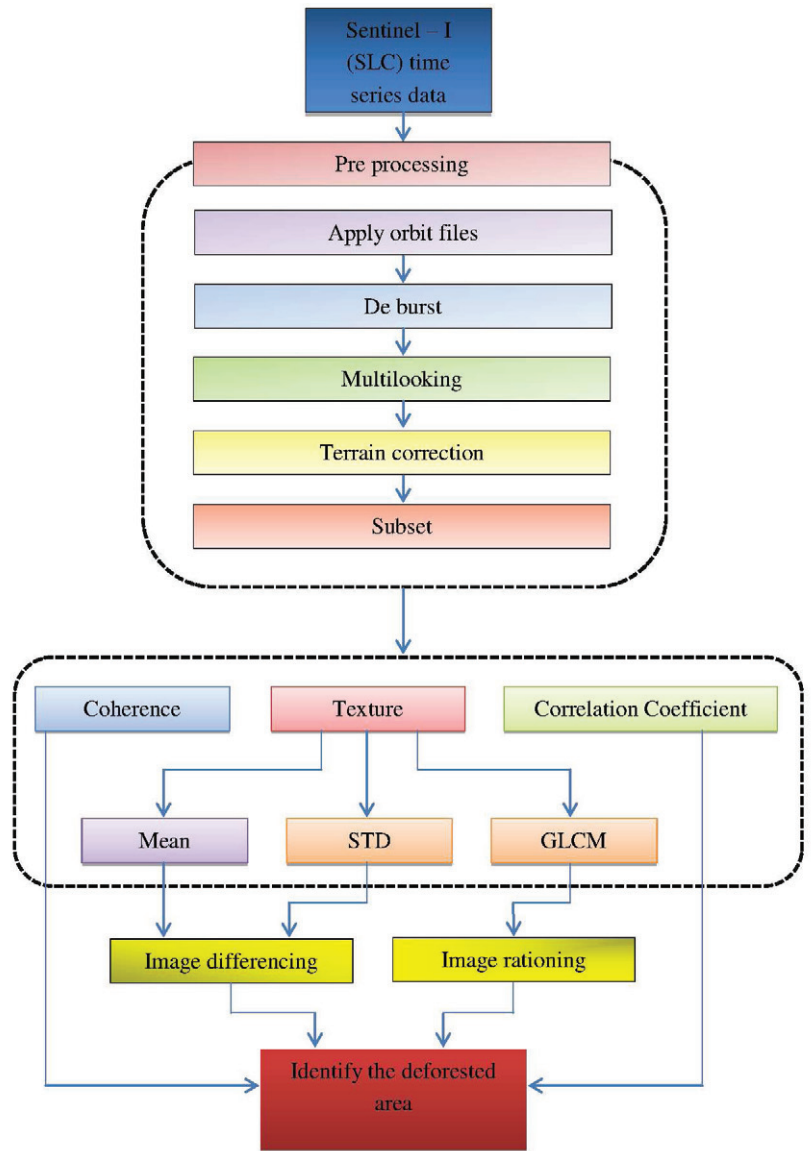


Figure 24: Flow chart for the Methodology

5.3. Preprocessing of Sentinel 1 Satellite Images

5.3.1. Apply orbit files

The orbit state vectors provided in the metadata of a SAR product are generally not accurate and can be refined with the precise orbit files which are available days-to-weeks after the generation of the product.

The orbit file provides accurate satellite position and velocity information. Based on this

information, the orbit state vectors in the abstract metadata of the product are updated. For Sentinel-1, restituted orbit files and precise orbit files may be applied. Precise orbits are produced a few weeks after acquisition. Orbit files are automatically download from Array's servers. If an orbit file is not found, looking for it in <https://qc.sentinel1.eo.esa.int/> and placing the downloaded file into the aux data folder.

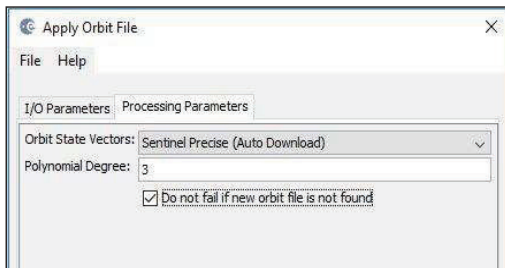


Figure 25: Apply orbit files

5.3.2. De burst

For the TOPSAR IW and EW SLC products, each product consists of one image per swath per polarization. IW products have 3 swaths and EW have 5 swaths. Each sub-swath image consists of a series of bursts, where each burst was processed as a separate SLC image. Thus it is necessary to Deburst these three sub swaths before they use for an application. This operation,

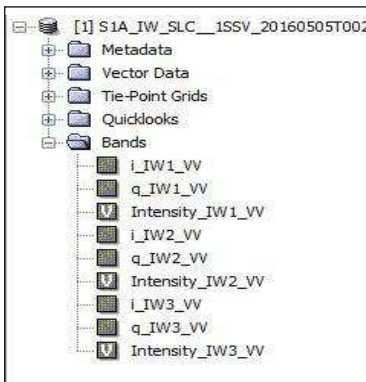


Figure 26: Before the Deburst

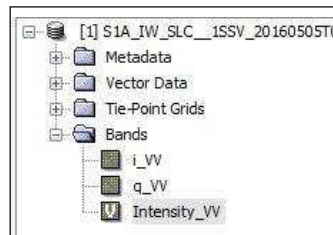


Figure 27: After the Deburst

Images for all bursts in all sub-swaths of an IW SLC product are re-sampled to a common pixel spacing grid in range and azimuth. Burst synchronization is ensured for both IW and EW products.

5.3.3. Multilooking

Generally, a SAR original image appears speckled with inherent speckle noise. To reduce this inherent speckled appearance, several images are incoherently combined as if they corresponded to different looks of the same scene. This processing is generally known as multilook processing. As a result the multilooked image improves the image interpretability. Additionally, multilook processing can be used to produce an application product with nominal image pixel size.

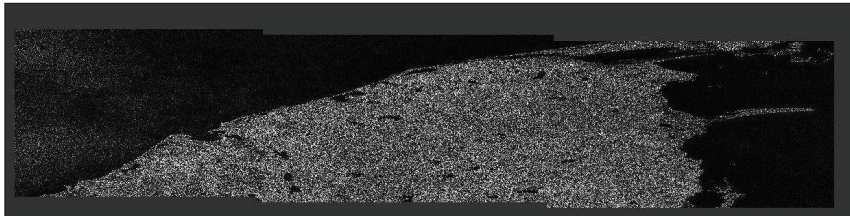


Figure 28: Before the Multilooking

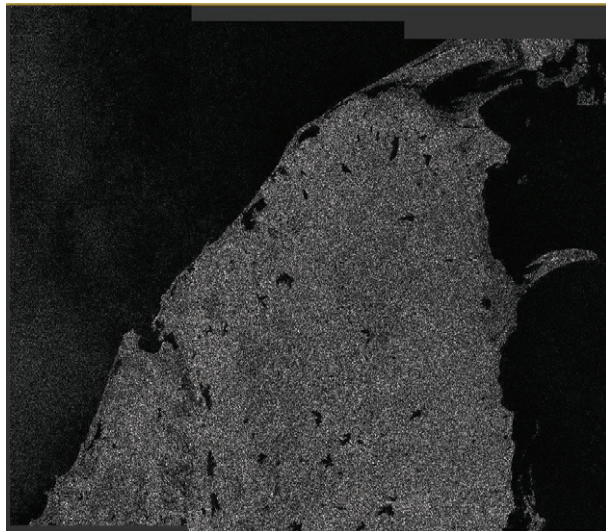


Figure 29: After the Multilooking.

5.3.4. Geocoding (Range Doppler Terrain Correction)

Due to topographical variations of a scene and the tilt of the satellite sensor, distances can be distorted in the SAR images. Image data not directly at the sensor's Nadir location will have some distortion. Terrain corrections are intended to compensate for these distortions so that the geometric representation of the image will be as close as possible to the real world.

Geocoded Imagery is a term which describes any remotely sensed imagery that has been transformed onto a cartographic projection (e.g., Universal Transverse Mercator, UTM) and is independent of both the sensor and the motion of the satellite platform from which the original raw imagery was collected. It does not imply that terrain effects have been taken into account. In general, the process involves the following operations:

1. Correction of geometric effects;
2. Registration to geographic co-ordinate systems;
3. Resampling to map scale and format without degradation of radiometric quality (<https://sentinel.esa.int/>, 12.05.2017).

Currently, only the DEMs with geographic coordinates (P_{lat} , P_{lon} , P_h) referred to global geodetic ellipsoid reference WGS84 (and height in meters) are properly supported for Terrain correction and Various different types of Digital Elevation models can be used. In this case SRTM 3 sec DEM's were used for the process.

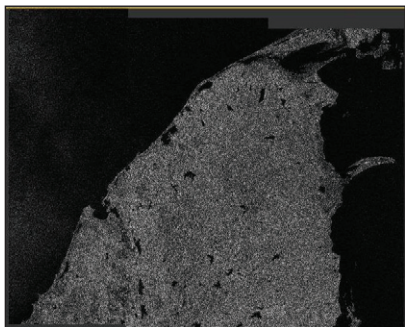


Figure 31: Before the Range Doppler Terrain
Correction



Figure 30: After the Range Doppler Terrain
Correction

5.3.5. Co registration

Co-registration is the process of superimposing multi-date, slant range images of the same area. Co-registered imagery is often a requirement to time-series filtering and processing of layer stacks. Accurate alignment of the two images, co-registration within small fraction of pixels.

The sub-pixel coregistration of SAR images is a strict requirement and critical component of any interferometric processing chain. It is an essential step for the accurate determination of phase difference, and applications such as DEM map

generation, interferometric deformation analysis, and the interferometric modules of the toolbox will accurately co-register one or more slave images with respect to a master image. The co-registration procedure is completely automatic.

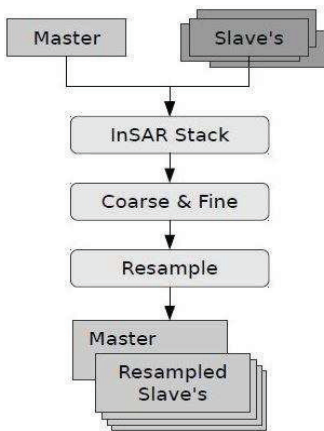


Figure 32: Overview of Coregistration Processing Chain

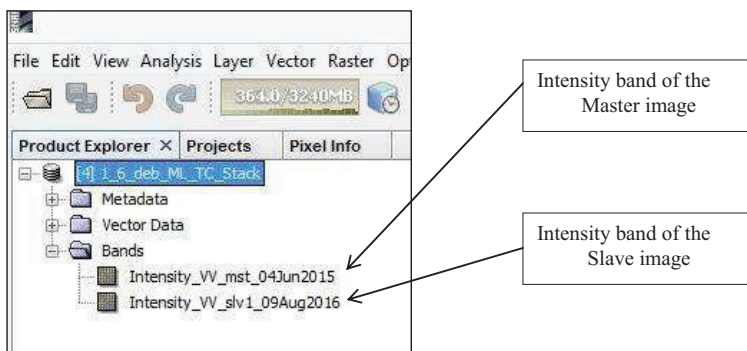


Figure 33: Geocoded Product

5.3.6. Subset

This operator is used for creating new product from a base product. It allows to subset an image in two ways, Using Pixel Coordinates and Geo coordinates.

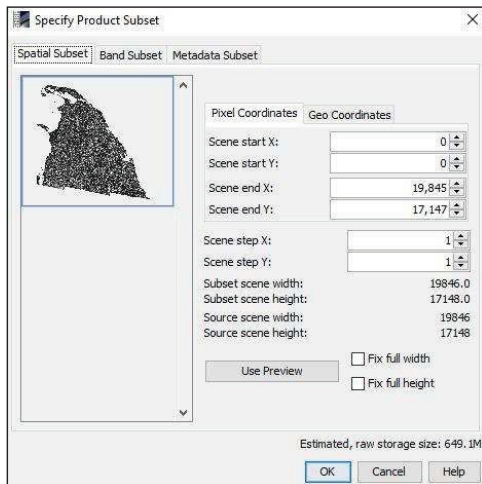


Figure 34: Subset tool

5.4. Graph builder

To pre-process images above mentioned procedures should be done one by one. It is very time consuming and difficult process. So Graph Builder has been introduced by SNAP software, it allows to process the image at once. The Graph Builder allows the user to assemble graphs from a list of available operators and connect operator nodes to their sources.

5.4.1. Graph of pre-process an image

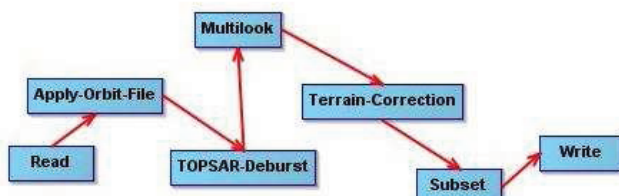


Figure 35: Image preprocessing steps in a single Graph operation

5.5. Extraction of deforested areas from RADAR images.

In order to extract the changes of the forest canopy following steps were executed,

1. The correlation coefficient,
2. Coherence
3. Using texture measure
4. The change detection by image rationing between pre-and post-event radar images,

The reduction of the correlation coefficient and coherence are mainly expected from the deforested area with some radar illumination changes but temporal behaviour of the volume scattering of forest canopy and vegetation patches can be expected as the temporal difference of two images.

Three separate graphs were produced to find the deforested area. Those graphs had been summarized below.

5.5.1. Graph for Coherence estimation

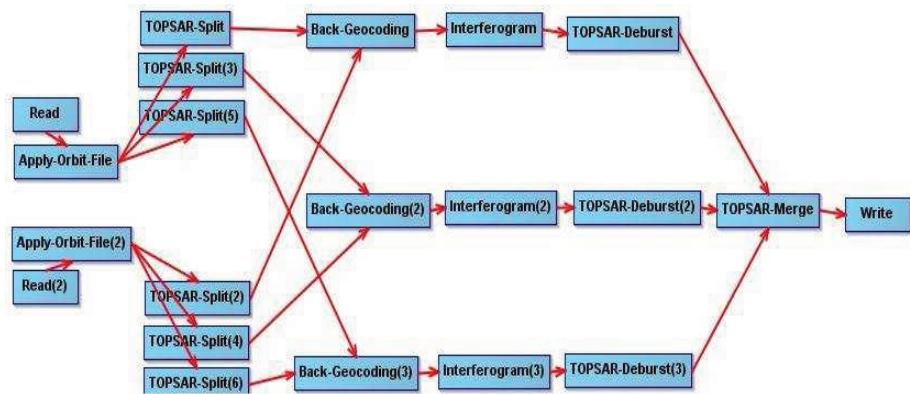


Figure 36: Coherence estimation

5.5.2. Graph for Change detection by image rationing

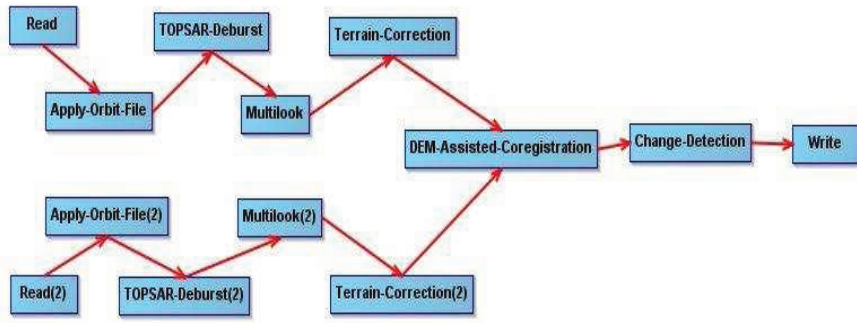


Figure 37: change detection by image rationing

5.5.3. The correlation coefficient

SNAP is not provided any pre-defined tool for calculating the correlation coefficient between two RADAR images. Because of the band math operator can be used to find the correlation between two RADAR images.

$$\text{Correlation} = \frac{(I_1 - \mu_1) * (I_2 - \mu_2)}{\sigma_1 * \sigma_2} \quad \dots \dots \dots \text{Equation 5.1}$$

μ is the Mean

σ is the Standard Deviation

I_1, I_2 is the pixel value of the image 1 and 2

Mean value and Standard Deviation of both 1st and 2nd images were calculated by Statics tool in SNAP.

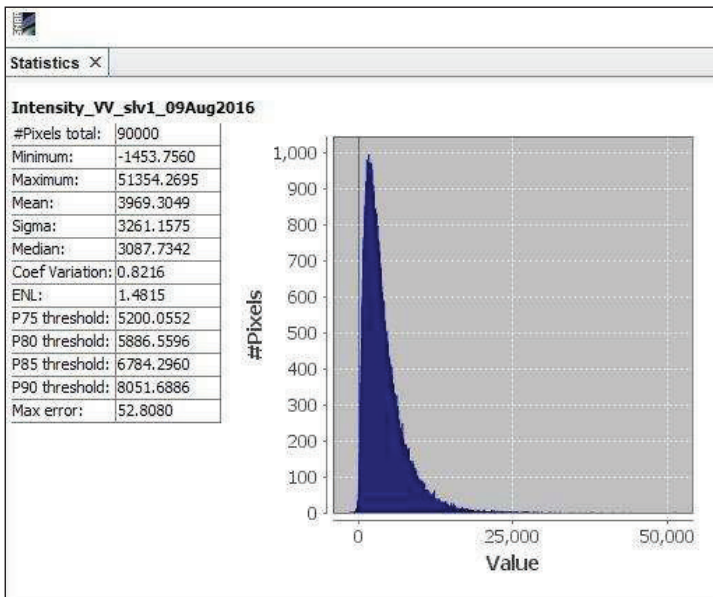


Figure 38: Statics for subset of 2016.09.26 image

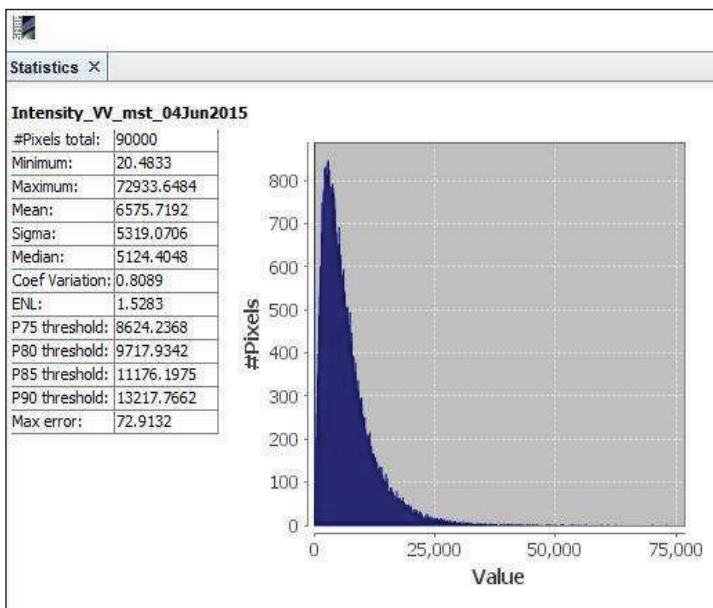


Figure 39: Statics for subset of 2015.06.24 image

The Equation used for Band Math operator,

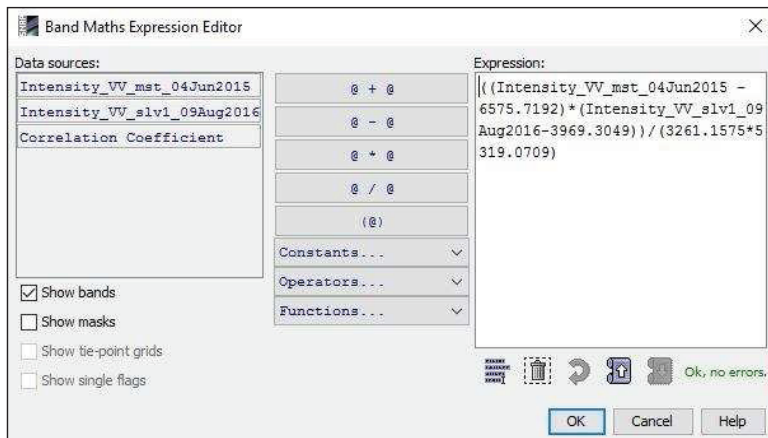


Figure 40: Correlation coefficient by Band Math operator

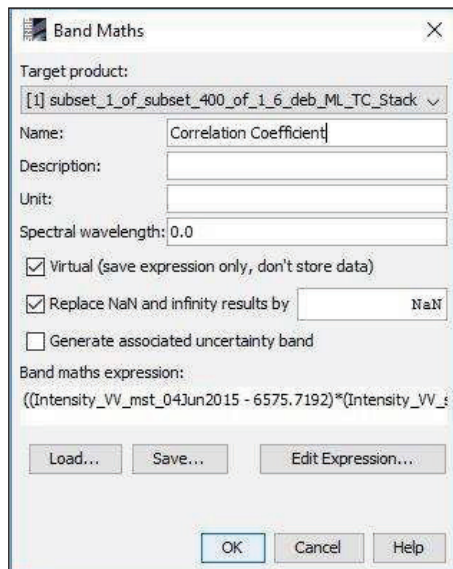


Figure 41: Band Math operator

5.6. Texture Analysis

For this it was used GLCM and Mean and Standard Deviation to produce 12 texture images. For more details, refer section 2.5.

Graph for Texture Analysis by GLCM.

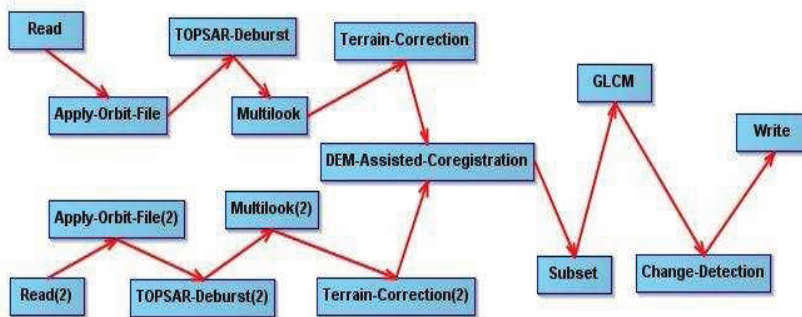


Figure 42: Graph for Texture analysis

6. Results and Discussion

Two data sets were downloaded as single polarization and dual polarization. The acquisition dates for those data sets were mentioned on chapter 4. The results obtained for both polarizations were lay head together.

6.1. Coherence Estimation.

The first objective of this study is estimating the amount of deforestation in Wilpattu by interferometric coherence technique. The results were obtained for Coherence estimation is as follows.

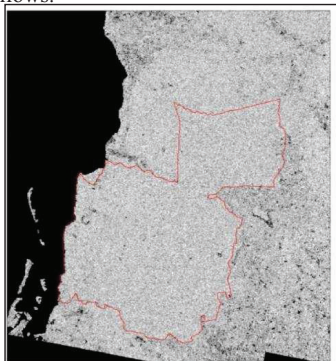


Figure 43: Coherence between images of 2016.06.04 and 2016.08.15 (VV Polarization)

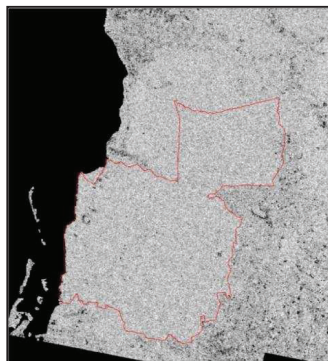


Figure 44: Coherence between images of 2016.06.04 and 2016.07.16 (VV Polarization)

[1, 2]

[1, 5]

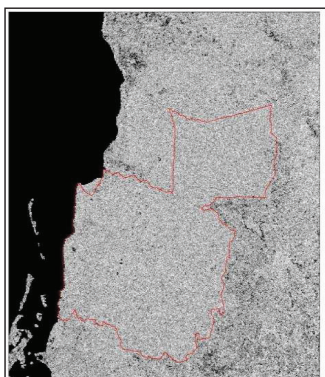


Figure 46: Coherence between images of 2016.06.04 and 2016.08.16 (VV Polarization)

[1, 6]

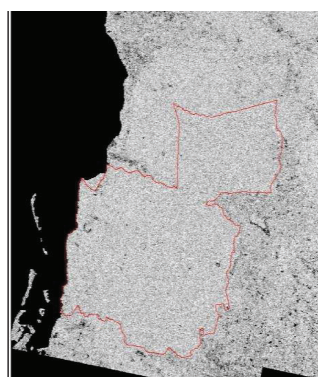


Figure 45: Coherence between images of 2016.03.18 and 2016.09.26 (VH Polarization) [1, 2]

- Wilpattu boundary
- Minimum Coherence
- Maximum Coherence (1)

The extent of change observed in each image is gradually increasing coherence images from Figure 43 to Figure 46. Here the coherence of the temporal SAR image pair will be analysed. As discussed earlier in chapter 2 the coherence will measure the correlation between the backscatter and the phase of the temporal image pair which may contain valuable information about the land cover. Coherence image can be used to find the changed areas because it gives high coherence values for unchanged areas and low coherence value for changed areas. For analysing the coherence value for the study area it was selected four regions from the coherence map as water, low forest cover, dense forest cover and deforested area. For the selection of these areas it was first prepared the shape files by digitizing Google earth image and then required regions were extracted from the coherence image.

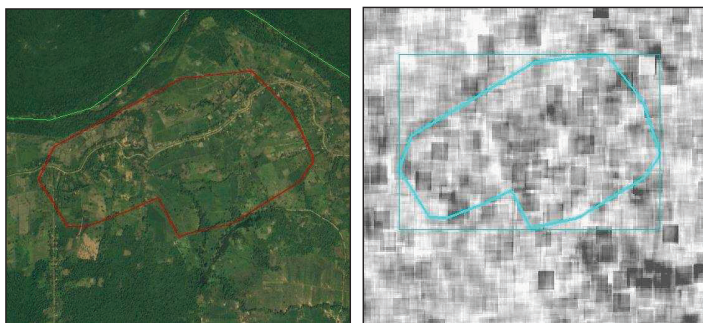


Figure 47: Low forest cover



Figure 48: Water

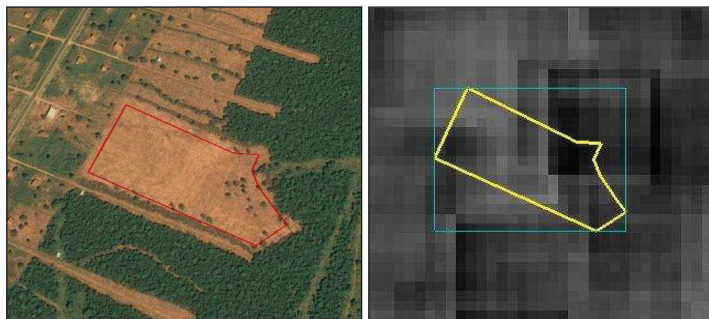


Figure 49: Deforested area

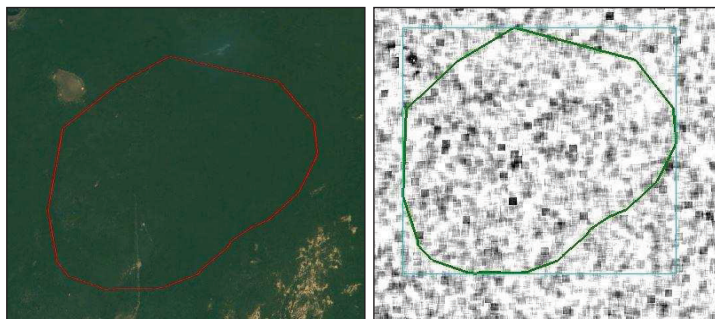


Figure 50: Dense forest cover

Then the Histogram for coherence (between two images acquired in 2016.06.04 and 2016.09.26) were plotted for the above four regions as shown below.

1. Histogram for Dense Forest Cover

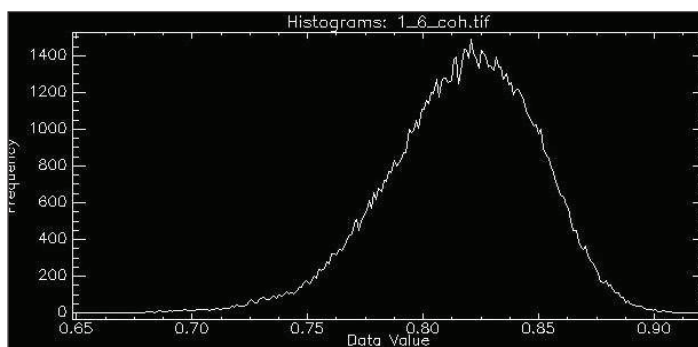


Figure 51: Histogram for dense forest cover

2. Histogram for Moderate Forest Cover

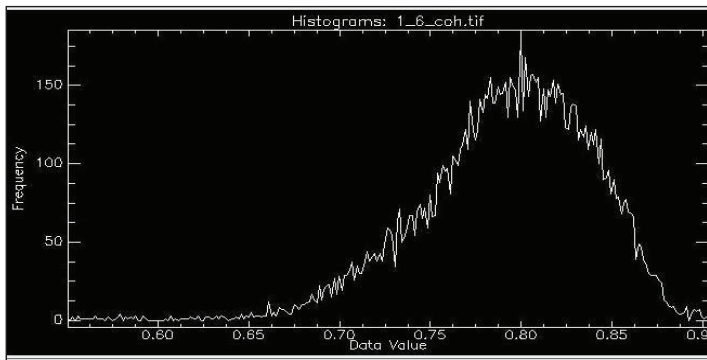


Figure 52: Histogram for moderate forest cover

3. Histogram for Water

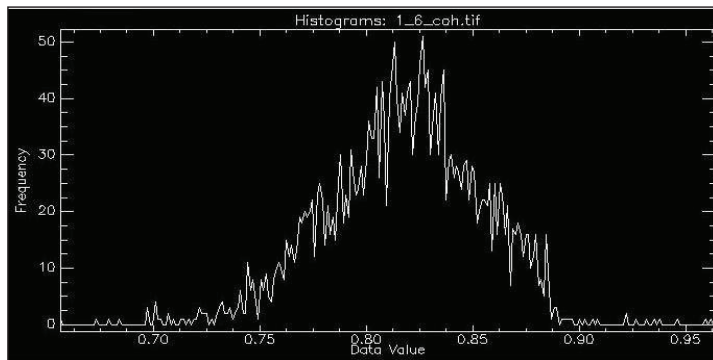


Figure 53: Histogram for Water

4. Histogram for Deforested region

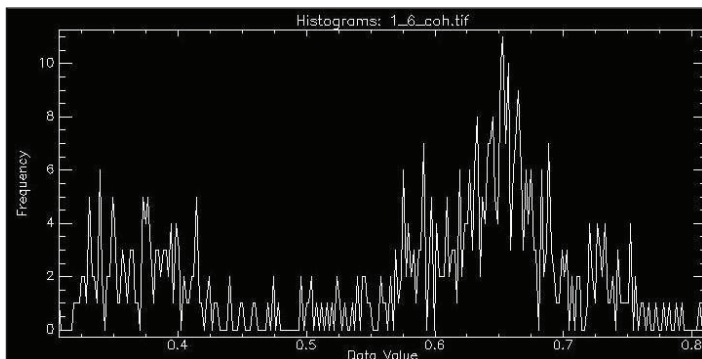


Figure 54: Histogram for Deforested area

When considering the above Histogram Coherence value for Water, Dense forest and low forest cover indicates a high coherence value than deforested regions. The following graph shows the mean coherence values for above selected areas,

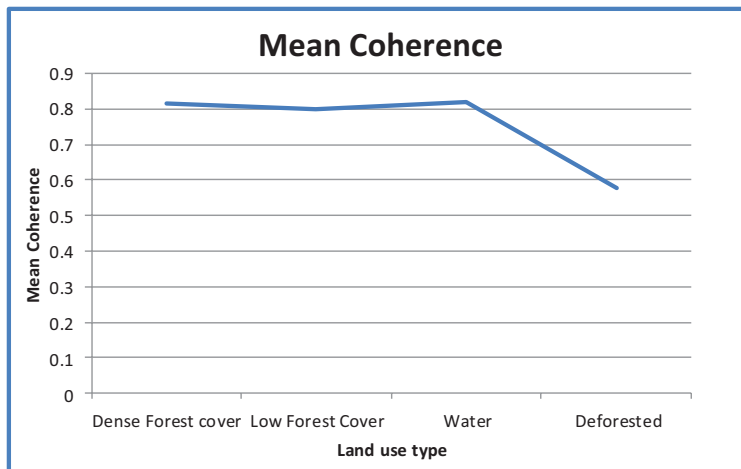


Figure 55: Mean coherence value for selected regions

Table 3: Coherence value for selected land use types

Land Use Type	Mean Coherence Value
Dense Forest cover	0.817105
Low Forest Cover	0.798732
Water	0.818211
Deforested	0.575552

In these Histograms it can be observed that there exists higher values for water, dense forest cover and low forest cover classes and lower values for deforested region. It is because prior to deforestation these areas were subjected mainly to a volume scattering and after deforestation the bare soil was subjected to surface scattering. In these two incidents the scattering mechanism is different and so it gives different backscatter values. This causes the low correlation between two incidents thus low coherence.

A high coherence can be observed only for unchanged areas. When it is considered the area within the boundary of Wilpattu National park, there also a high coherence exists. So this area can be considered as an unchanged area. But this coherence value is not equal to 1, since theoretically forest cover has less coherence value due to their temporal behaviour and because of the temporal decorrelation of two data sets used for the analysis.

The histogram for the coherence image is as follows,

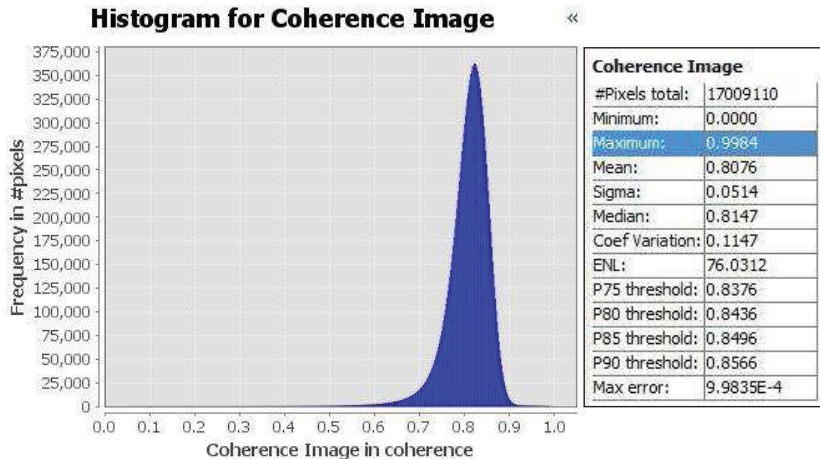


Figure 56: Histogram for Coherence

Graphical plot for the coherence shows that the overall coherence of the image were high value and the distribution has a maximum frequency around 0.7 to -0.9 More than 95% of the pixels represents this area ,this is concluding that the study area had a minimum alteration during the study period.

6.2. Change detection Estimation

Image rationing method was used for change detection estimation this method was discussed in previous chapter. Theoretically in rationing, the black colour represents the unchanged areas while white colour represents changed areas. So accordingly there is limited deforestation within the boundary of Wilpattu and a significant amount of deforestation outside of the boundary.



Figure 57: Change detection between images of 2016.06.04 and 2016.08.15 (VV Polarization) [1, 2]

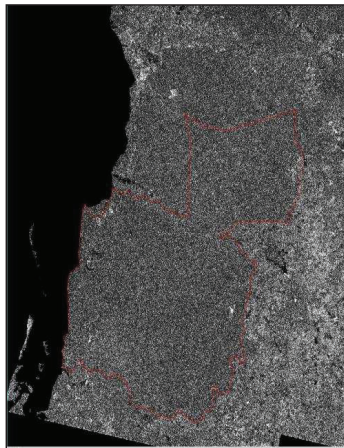


Figure 58: Change detection between images of 2016.06.04 and 2016.07.16 (VV Polarization) [1, 5]

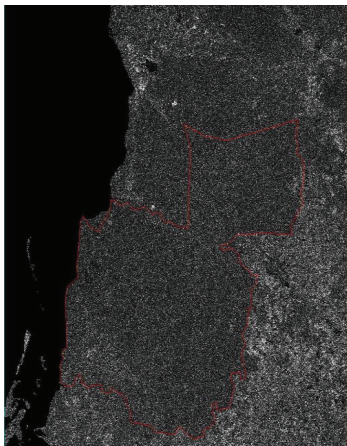


Figure 59: Change detection between images of 2016.06.04 and 2016.08.09 (VV Polarization) [1, 6]

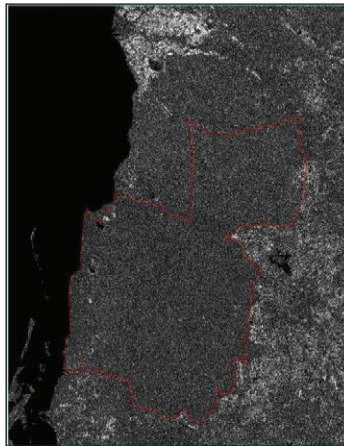


Figure 60: Change detection between images of 2016.03.18 and 2016.09.26 (VH Polarization) [1, 2]

- Wilpattu
- No change
- Maximum Change

According to the data represented by sentinel I (SAR) C band images; there is a very limited deforestation which is not strongly significant inside the boundary of Wilpattu National Park. But it can be observed some deforestation outside the boundary of Wilpattu. This was concluded according to the results of Coherence and Change detection methods.

Therefore it was attempted to identify accurately a deforested area outside Wilpattu boundary using the nature of the backscatter coefficient. Image obtained from the pre-processing of the image 2016.09.26 was used for backscatter analysis

The same shape files which were used in coherence analysis were used for this experiment. The observed graphical plots are as follows,

1. Histogram for Dense Forest Cover

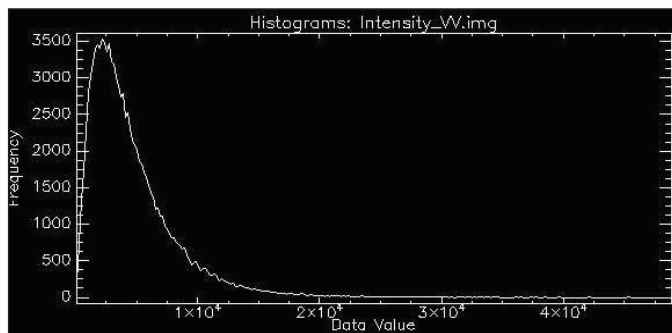


Figure 61: Histogram for Dense forest

2. Histogram for Low Forest Cover

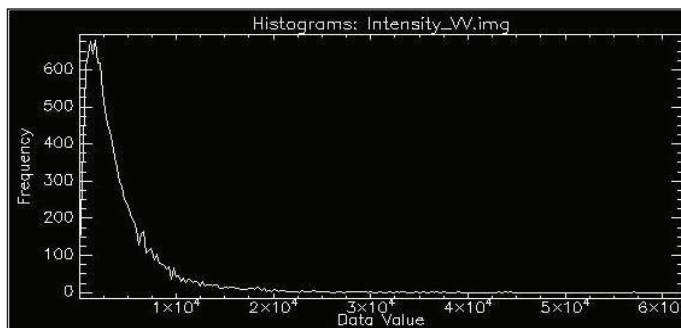


Figure 62: Histogram for Low forest Cover

3. Histogram for Water

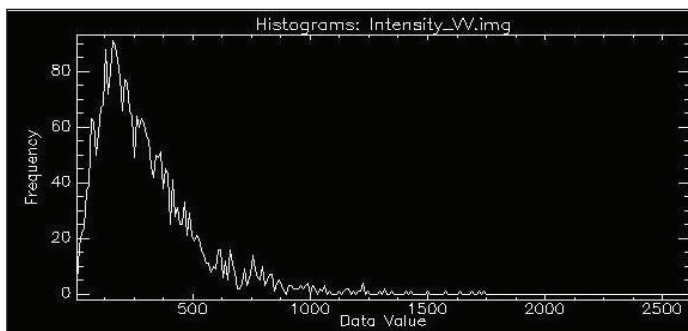


Figure 63: Histogram for Water

4. Histogram for Deforested area

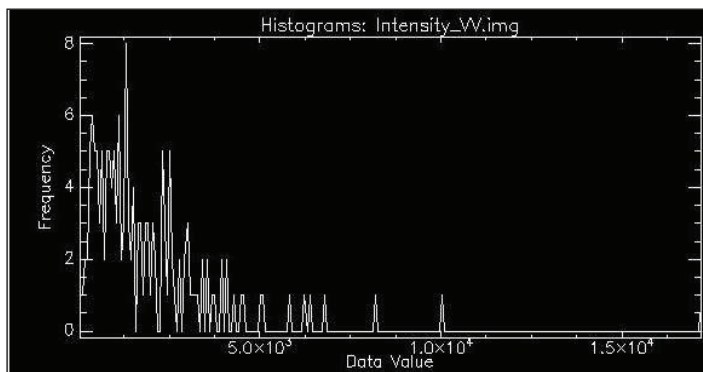


Figure 64: Histogram for Deforested area

The following graph shows the Mean backscatter value obtained for these Histograms.

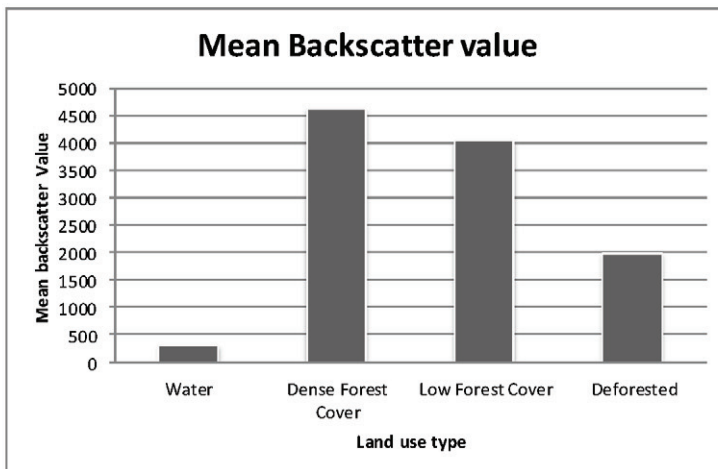


Figure 65: Mean backscatter for selected regions

Table 4: Mean backscatter value of selected land use types

Land Use Type	Mean Backscatter Value
Dense Forest cover	304.888
Low Forest Cover	4619.2247
Water	4043.23
Deforested	1979.549

By carefully observing the above graph it can be noted that the mean backscatter for deforested regions are lower than the both dense and low cover forest regions. The reason behind this observation could be the loss of the volume scattering effect due to the canopy removal or changes with the deforestation.

And also the backscatter value for water indicated a low value relative to other study regions. The reason for this is the phenomenon of Specular Reflection where water acts like a specular reflector due to the dielectric properties of the water. Due to the smoothness of the water bodies it will be deflected all the RADAR waves reaching its surface out of the receiving antenna thus have low backscatter energy to the radar image comparing to the background features.

6.3. Texture Analysis

When it is compared the results of coherence estimation and change detection, it can be observed a similarity in the results of both procedures. As discussed in earlier in both result sets limited deforestation can be observed in the area within the boundary of Wilpattu. So it was analysed an area beyond the boundary of Wilpattu using Texture analysis and Correlation Coefficient in order to observe the nature of the backscatter coefficient of an area with deforestation. Two data sets were selected; 2016.06.04 as pre image and 2016.08.09 as post image to be analysed in Matlab and GLCM for Texture analysis.



Figure 66 : Google Earth image for selected deforested area

The following images were obtained by subsetting the original image using the coordinates of google earth image.

6.3.1. MATLAB processing for texture analysis

The figure 67 and 68 shows the subset image of the RADAR images which were used in order to extract the texture images.

The following textures were derived by executing respective MATLAB codes (Appendix) for the original image.

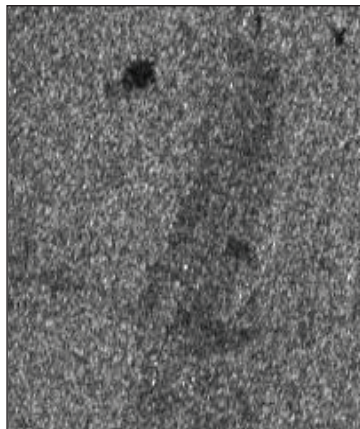


Figure 67: Subset of image 1 (2016.06.04)

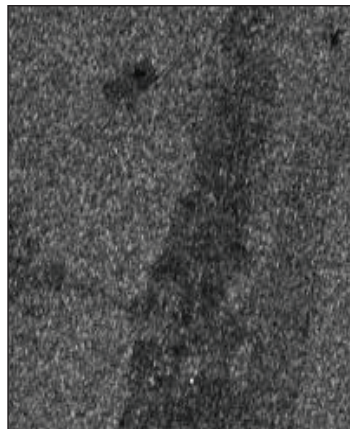


Figure 68: Subset of image 6 (2016.08.09)

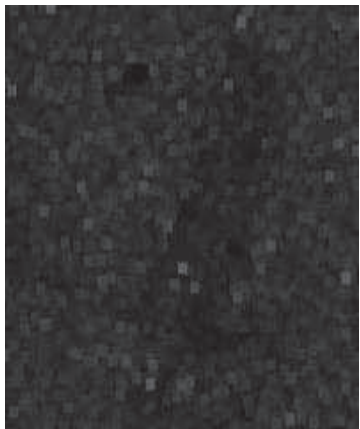


Figure 69: Standard Deviation texture of
image 1 (2016.06.04)

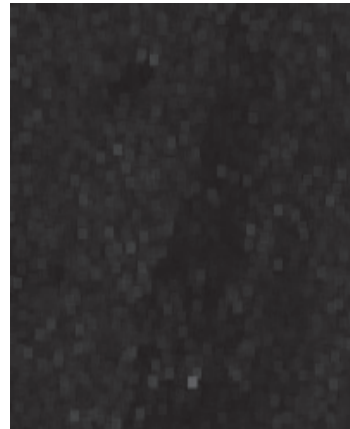


Figure 70: Standard Deviation texture of
image 6 (2016.08.09)

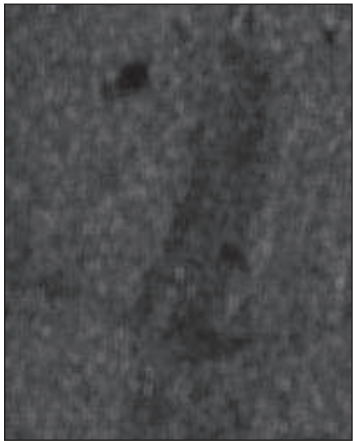


Figure 72: Mean texture of image 1
(2016.06.04)

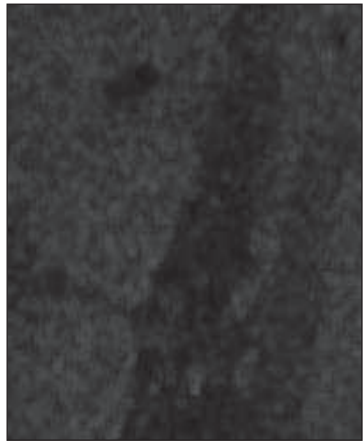


Figure 72: Mean texture of image 6
(2016.08.09)

Though it can be observed a considerable backscatter variation in the original image for canopy and bare soil, in the obtained Mean and STD texture images it was unable to observe a considerable backscatter strength variation. It is because, the above images obtained as Mean texture and Standard deviation texture represent less scattering variations. It can be due to smoothing of the RADAR image during Mean and STD texture image formation and due to the change of values of the all pixels according to the deforestation of the area causing an elimination of the effect of the mean.

6.3.2. GLCM Analysis

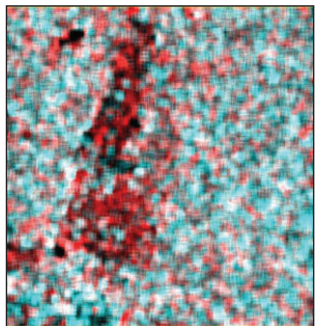
The results of the texture analysis done in SNAP, GLCM were subjected to RGB visualization in order to distinguish the bare soil and canopy. The RGB visualized texture images were as follows.

RGB visualization in Figure 73 has the following color combinations.

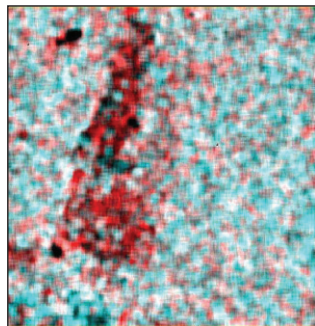
Red: Post Texture image - 09.08.2016

Green: Pre Texture image - 04.06.2015

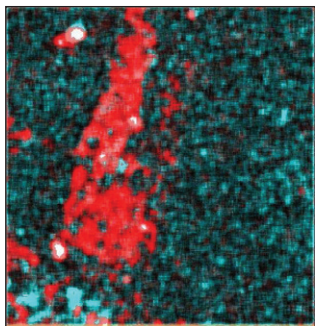
Blue: Pre Texture image - 04.06.2015



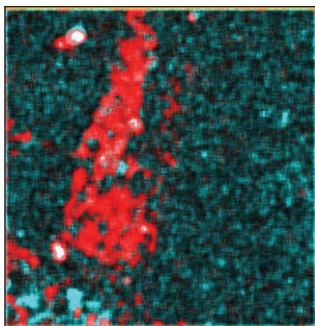
RGB visualization of Contrast
texture



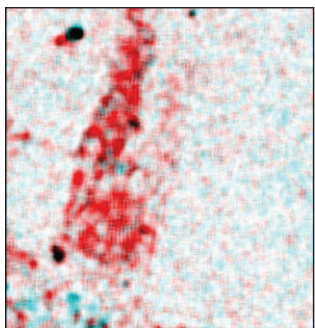
RGB visualization of
Dissimilarity texture



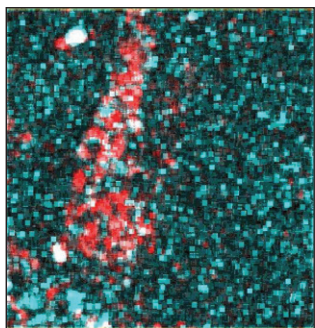
RGB visualization of Energy
texture



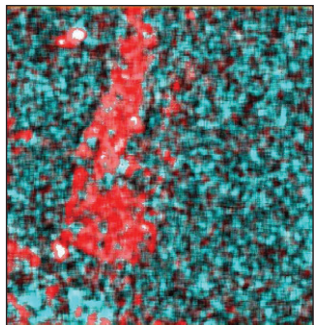
RGB visualization of ASM
texture



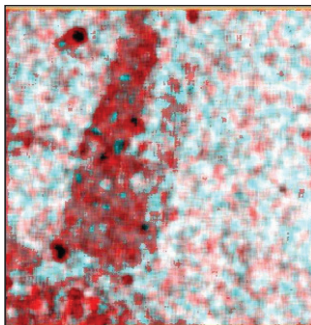
RGB visualization of Entropy
texture



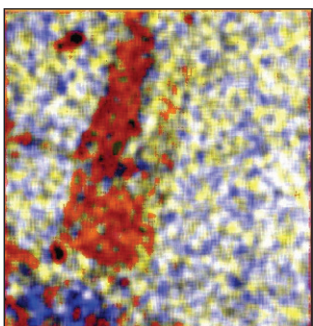
RGB visualization of Max
texture



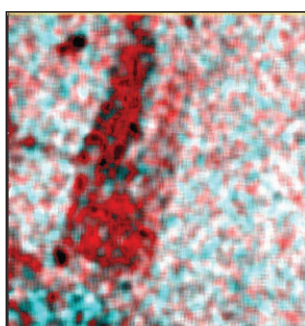
RGB visualization of
Homogeneity texture



RGB visualization of GLCM
Correlation texture



RGB visualization of GLCM
Variance texture



RGB visualization of GLCM
Mean texture

Figure 73: RGB Visualizations of Texture images derived for images acquired on
2015.06.04 and 2016.08.06

This combination can be used to distinguish between areas that are related to the bare soil and canopy. The areas which were altered during this time period are represented in Red as the post image was selected for the red channel, while the white colour depicts the area where no change had been occurred which means that the backscatter of the area is same. So the red patches in texture images were corresponding to the bare soil and other area representing the canopy cover. Though in theoretically, the regions which are not related to the bare soil should be in white colour, (since there is no any change had been occurred in those areas) they were not, because of the temporal behaviour of the forest canopy and temporal decorrelation of two data sets used for the analysis.

Based on a visual study of the above results it was clear that the most appropriate texture for the identification of deforestation is Entropy and ASM (Angular Second Moment). Then the next experiment was to find the appropriate method statically for that, the respective images obtained in RGB visualization were used to mask out the bare soil. Then the areas of each mask out region were calculated. The table 5 below shows the resulted area from texture images.

Table 5: Calculated area for different texture images

Texture image	Area (Km ²)	Area Difference
Max	2.061	-0.7832115
Contrast	1.300	-1.5442115
ASM	2.996	0.1517886
Entropy	3.126	0.2817886
Energy	3.290	0.4457886
GLCM Correlation	4.206	1.3617886
GLCM Variance	3.195	0.3507886
GLCM Mean	1.602	-1.2422115
Homogeneity	2.865	0.0207886
Dissimilarity	4.964	2.1197886
Energy	3.290	-0.7832115

Actual area of the bare soil was calculated by digitizing the Google earth image because the time and cost allocated for the research limited the field observations. The obtained rough area was 2.84421145 km². Detected bare soil areas are numerically compared with the area derived from Google earth. The comparison of these results shows that Homogeneity texture image is more suitable to detect the bare soil from forest area and the error for the area is 0.0207886 km² the Entropy and ASM also gives better results for the statistical analysis. The graph for the deviations is as follows,

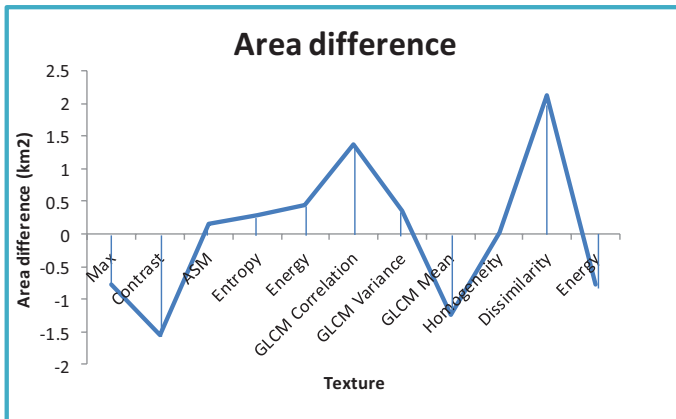
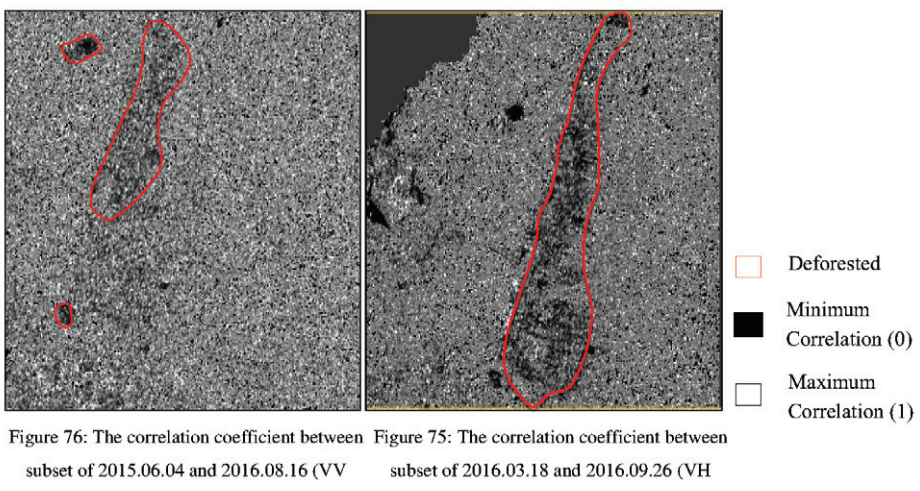


Figure 74: Area difference for different texture images

The negative values of the graph shows the areas where the obtained area is less than the actual value while the positive values shows the areas where the obtained area is higher than the actual value. Therefore according to this analysis it can be shown that Max, Contrast, GLCM Mean and Energy are texture images representing the areas less than the actual value and ASM, Entropy, Energy, GLCM Correlation, GLCM Variance, Homogeneity and Dissimilarity are texture images representing the areas higher than the actual value.

6.4. Correlation coefficient

In order to extract the changes due to the deforestation, the correlation coefficient and the difference between two radar images were calculated for Wilpattu area. The reduction of the correlation coefficient is mainly expected from the damaged area with some radar illumination changes. Seasonal changes of forest canopy and vegetation patches can influence to the results since the temporal difference of two images being higher than one year. The results were obtained for Correlation coefficient is as follows.



It is obvious that, the area detected from co polarizing approach provides the least percentage of accuracy than cross polarizing approach, because as mainly the volume scattering within a forest canopy is highly sensitive to the cross polarization which is effect on RADAR images than the co polarization.

Figure 77 shows the relationship between the correlation and difference of two radar images before and after the event by examining the characteristics of radar backscatter values in altered deforested area. In theoretically, if any changes of geographical phenomena were occurred in between these two image acquisitions, the less correlation (< 0) or minus relations have been defined the change.

By using backscatter analysis, it can be concluded that the area was damaged consists low backscatter value than the canopy area. Hence, the backscatter value is decreasing from 2015.06.04 image to 2016.08.16 image. So, even the difference between images represents a minus value and that is describing about the changes of the areas. By considering above two concepts, change pixels were extracted by selecting the minus areas of the scatter plot (Figure 77) by the Region of Interest (ROI). The possible range of deforestation is interpreting between the correlation coefficient vs. difference and the extracted deforested areas after masking are illustrated Figure 78.

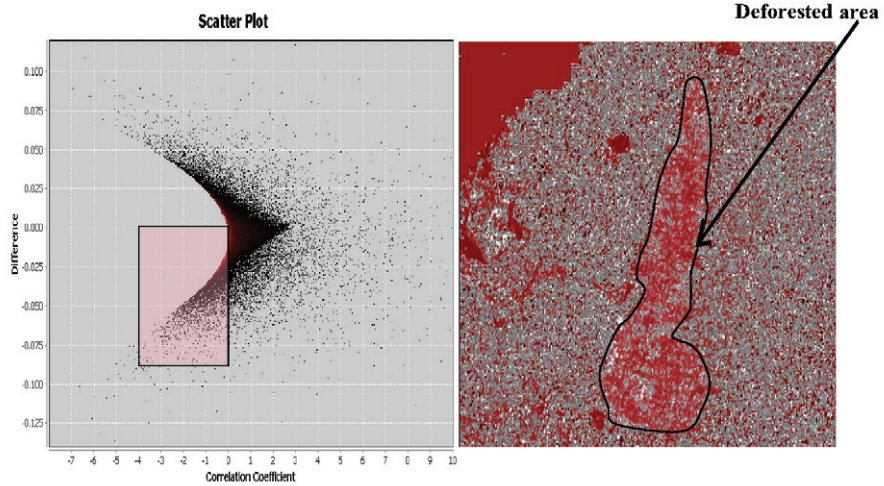


Figure 78: Scatter plot between correlation coefficient and Difference image for VH polarization pre and post images.

Figure 78: Extracted deforested areas from the scatter plot of Difference image for VH polarization pre and post images.

The correlation between change detection methods and texture images were calculated by using statistical analysis tool in Arc GIS 10.1. It appeared that there were high correlations between image difference and the correlation coefficient with texture images while the correlation between Coherence and image rationing were very small.

Table 6: The correlation between change detection methods and texture images

	Complex Coherence	Image rationing	Correlation Coefficient	Image Difference
Contrast	0.14490	0.07979	0.33804	0.30518
GLCM Covariance	0.01676	0.11833	0.23634	0.28444
Energy	-0.17517	-0.13440	-0.49700	-0.42481
Entropy	0.15050	0.18993	0.35766	0.28965
Homogeneity	-0.05361	-0.07818	-0.21257	-0.21571
Max	-0.12747	-0.07119	-0.22993	-0.21103
GLCM Mean	0.12002	0.13281	0.35090	0.41977
GLCM Variance	0.14133	0.11819	0.34636	0.39384
Dissimilarity	0.12828	0.08791	0.35377	0.32241
ASM	-0.17079	-0.10498	-0.35701	-0.32576

When consider about the highest value which are represented in Complex Coherence, Image rationing and Correlation Coefficient, that have given by Entropy. So it can be concluded that Entropy is most suitable to identify the deforested area by using these three change detection methods.

7. Conclusion

In this research, the main objective was to detect deforested areas in Wilpattu from radar remote sensing techniques by applying different change detection methods. Basically, complex coherence, correlation coefficient, image differencing and images rationing techniques were applied for two sentinel 1 SAR C band images before and after the event. There is a very limited deforestation which is not strongly significant inside the boundary of Wilpattu National Park. But it can be observed some deforestation outside the boundary of Wilpattu. This was concluded according to the results of Coherence and Change detection methods.

Texture analysis was concluded that Entropy is most suitable to identify the deforested area since it gives the highest correlation with change detection methods.

The interaction of RADAR signal with the real earth features as dense vegetation cover, deforested and water is different to each other. By taking this fact in consideration, back scatter analysis was performed. The results showed that mean backscatter for deforested regions is lower than the both dense and low cover forest regions and the backscatter value for water indicated very low value relative to other study regions due the phenomenon of Specular Reflection.

Finally results of the study proving that the single polarization C-band RADAR imageries were capable of estimating the deforestation in area, but results may depend on several factors including the following.

1. Precise geometric registration between multi-temporal images
2. Calibration or normalization between multi-temporal images
3. Availability of quality ground truth data
4. The complexity of landscape and environments of the study area
5. Change detection methods or algorithms used
6. Classification and change detection schemes
7. Analyst's skills and experience
8. Knowledge and familiarity of the study area
9. Time and cost restrictions.

8. Reference

Brandt TSO, Paul M. Mather, 2000, Classification Methods For Remotely Sensed Data Second Edition, Boca Raton, FL 33487-2742, pp 1 -38.

Dahdal B., 2011, The use of interferometric space borne RADAR and GIS to measure peat subsidence in Indonesia, University of Leicester, pp 113-114

Giri Tejaswi, March 2007 , Manual On Deforestation, Degradation, And Fragmentation Using Remote Sensing And Gis, Strengthening Monitoring, Assessment And Reporting On Sustainable Forest Management In Asia (Gcp/Int/988/Jpn), pp 5-6

<http://www.nrcan.gc.ca/earth-sciences/geomatics/satellite-imagery-airphotos/satelliteimager-products/educational-resources/9341>

Kariyawasam K.M.H.R. , Rajapakse C., July 2014, Impact of Development on deforestation in Sri Lanka: An analytical study, IOSR Journal of Environmental Science, Toxicology and Food Technology (IOSR-JESTFT) e-ISSN: 2319-2402,p- ISSN: 2319-2399.Volume 8, Issue 7 Ver. II (July. 2014), PP 35-39

NRCAN, RADAR Polarimetry Retrieved February 18, 2017, from <http://www.nrcan.gc.ca/earth-sciences/geomatics/satellite-imagery-air-photos/satelliteimager-products/educational-resources/9275>

NRCAN, Viewing Geometry and Spatial Resolution , Retrieved January 08, 2017, from Rahman M.M., 2010, Mapping tropical forest cover and deforestation using synthetic aperture radar (SAR) images, at Springerlink.com pp 113-121

Ranasinghe A. K. R. N., Sirisenal P. M. T. S., Dammalage T. L., Puswewala U. G. A.,2016, INTEGRATION OF RADAR AND OPTICAL REMOTE SENSING FOR LANDSLIDE DETECTION - A CASE STUDY OF MEERIYABEDDA LANDSLIDE IN SRI LANKA, 37th Asian Conference on Remote sensing, Colombo, Sri Lanka

Samuel W., Jackson C.R., September 2004, Principle of Synthetic Aperture Radar, SAR Marine users' Manual, NOAA/NESDIS , pp 1-23

Sentinel1 user Handbook Retrieved January 15, 2017, from <https://sentinel.esa.int/>

Vyjayanthi N., Jha C. S., Murthy M. S. R., Yadav D.K., Singh L. October, 2008, Forest Biomass Estimation and Forest Structure Analysis of Deciduous Forests Using SAR Data, Indian Space Research Organization, Hyderabad ,pp 1 -14

A black and white photograph of a young woman with long, dark hair, smiling while reading an open book. She is wearing a light-colored cardigan over a dark top. The background is slightly blurred.

yes

I want morebooks!

Buy your books fast and straightforward online - at one of the world's fastest growing online book stores! Environmentally sound due to Print-on-Demand technologies.

Buy your books online at
www.get-morebooks.com

Kaufen Sie Ihre Bücher schnell und unkompliziert online – auf einer der am schnellsten wachsenden Buchhandelsplattformen weltweit!
Dank Print-On-Demand umwelt- und ressourcenschonend produziert.

Bücher schneller online kaufen
www.morebooks.de

SIA OmniScriptum Publishing
Brivibas gatve 1 97
LV-103 9 Riga, Latvia
Telefax: +371 68620455

info@omnascriptum.com
www.omnascriptum.com



